Advanced binary guanosine and guanosine 5-monophosphate cell-laden hydrogels for soft tissue reconstruction by 3D bioprinting.

Maria Godoy-Gallardo[†,]*, Maria Merino-Gómez[†], Miguel A. Mateos-Timoneda[†], Ulrich Eckhard[#], F. Javier Gil[†], Roman A. Perez[†,]*

[†]Bioengineering Institute of Technology (BIT), International University of Catalonia (UIC), Carrer de Josep Trueta, 08195, Sant Cugat del Vallès, Barcelona, Spain

[#]Department of Structural and Molecular Biology, Molecular Biology Institute of Barcelona (IBMB), Higher Scientific Research Council (CSIC), Barcelona Science Park, Baldiri Reixac 15-21, 08028 Barcelona, Spain.

ABSTRACT. Soft tissue defects or pathologies frequently necessitate the use of biomaterials that provide the volume required for subsequent vascularization and tissue formation, as autrografts are not always a feasible alternative. Supramolecular hydrogels represent promising candidates because of their 3D structure, which resembles the native extracellular matrix, and their capacity to entrap and sustain living cells. Guanosine-based hydrogels have emerged as prime candidates

in recent years, since the nucleoside self-assembles into well-ordered structures like G4-quadruplexes by coordinating K^+ ions and π-π stacking, ultimately forming an extensive nanofibrillar network. However, such compositions were frequently inappropriate for 3D printing due to material spreading and low shape stability over time. Thus, the present work aimed to develop a binary cell-laden hydrogel capable of ensuring cell survival while providing enough stability to ensure scaffold biointegration during soft tissue reconstruction. For that purpose, a binary hydrogel made of guanosine and guanosine 5-monophosphate was optimized, rat mesenchymal stem cells were entrapped, and the composition bioprinted. To further increase stability, the printed structure was coated with hyperbranched polyethylenimine. SEM studies demonstrated an extensive nanofibrillar network, indicating excellent G4-quadruplex formation, and rheological analysis confirmed good printing and thixotropic qualities. Additionally, diffusion tests using FITC-dextran (70, 500, and 2000 kDa) showed that nutrients of various molecular weights may diffuse through the hydrogel scaffold. Finally, cells were evenly distributed throughout the printed scaffold, cell survival was 85% after 21 days, and lipid droplet formation was observed after 7 days under adipogenic conditions, indicating successful differentiation and proper cell functioning. To conclude, such hydrogels may enable the 3D bioprinting of customized scaffolds perfectly matching the respective soft tissue defect, thereby potentially improving the outcome of the tissue reconstruction intervention.

1. INTRODUCTION

Hydrogels have gained increasing attention in tissue engineering due to their physicochemical properties, water-retention and drug loading capability, biocompatibility, and their implementable functionalities such as self-healing, shape memory, and bioactivity. These three-dimensional (3D) hydrophilic polymeric networks mimic soft tissues and can hold large amounts of water through

their network of entangled fibers. Molecular hydrogels, a subclass of hydrogels, are built from small molecules known as low-molecular-weight gelators, including many biocompatible and biodegradable compounds like peptides, sugars, lipids, and nucleosides/nucleotides.[1–4] These molecules interact through supramolecular interactions like hydrogen bonding, π-π stacking, metal-ligand coordination, or electrostatic and hydrophobic interactions.[5] Due to their flexibility, tenability, reversibility, and self-healing properties, they form soft hydrogels that are ideal for wound healing,[6] tissue engineering,[7] 3D cell culture,[8] and drug delivery applications.[9]

During gelation, the molecular building blocks initially form nuclei, which then grow and mature into ordered aggregates and nanofibers, and eventually cross-link or entangle to create a densely connected network that replicates the supramolecular interactions found in the extracellular matrix. Such biomimetic hydrogels, including those formed by guanosine (Guo) and its derivatives, have gained increasing popularity due to their simple composition and intrinsic biocompatibility. They possess both hydrogen donor and acceptor groups, allowing the formation of cyclic planar rings known as G-quartets (Scheme 1) via Hoogsteen base-pairing in the presence of monovalent metal cations such as potassium (K^+).[10] These G-quartets can further associate into columnar structures known as G-quadruplex (G4) through π-π stacking and sharing of the central metal ion. The involved quartets exhibit a rotation of approximately 30 degrees in relation to one another, resulting in a four-stranded, right-handed helical structure.[11] These mechanisms enable the self-assembly of Guo-based molecules into well-ordered structures and dynamic gels.[1,12–17] However, the potential application of these hydrogels is currently limited due to their restricted lifetime stability.[18–20] To overcome these limitations, various strategies have been explored to improve the stability and functionality of Guo-based hydrogels for tissue engineering.[13,21,22] One prominent approach involves the use of boronic acids (BAs).[19,22–24] Notably, Guo-borate ester hydrogels (GB)

have been found to result in stronger hydrogels compared to these without borate, highlighting the importance of the borate diesters presence for stable hydrogel formation.[17] Over the years, various structures based on GB hydrogels have been studied.[14,25–27] For instance, Peter *et al*.[28] demonstrated the importance of the right balance balance of BA and K^+ for both the gelation process and structural stability.

Alternatively, modifying the 5'-OH of Guo, such as using 5'-monophosphate[10,29,30] or 5'-hydrazides[31], has been suggested to improve the properties of Guo hydrogels. Belda *et al*.[32] investigated the self-assembly of guanosine 5'-monophosphate (GMP) derivatives using polyamines, which enhanced the stability of the resulting 3D network. Additionally, Zhang *et al*.[12] utilized a combination of hyperbranched polyethylenimine (PEI) and GMP as building blocks for G4 formation, resulting in gels with additional self-organization at pH ~4 due to the interaction between PEI's - NH_2 groups and GMP's phosphate groups.

Binary hydrogels composed of Guo and GMP have been extensively characterized, with properties varying on the Guo/GMP ratio.[11,13] At room temperature (RT) and neutral pH, GMP and Guo alone are either too soluble or insoluble, respectively, for proper gelation and formation of stable hydrogels. However, Guo/GMP mixtures[11,13] have demonstrated that GMP aids in the solubilization of Guo, while Guo's insolubility enhances the gelation of GMP even at low concentrations. For example, Carducci *et al*.[11] synthesized a transparent hydrogel with K^+ by combining Guo and GMP. Similarly, Nava *et al*.[13] investigated the gelation mechanism and reported the formation of a binary hydrogel composed of Guo and GMP, exhibiting a nano-partitioning phenomenon with distinct G-quartet columns and knotted G4 coils for 5-GMP-rich and Guo-rich regions, respectively. However, limited research has been done to evaluate their

performance in 3D-(bio)printing, likely due to material spreading issues after printing. Thus, further research is needed to optimize printability and thus applicability of these hydrogels.

3D printing offers a versatile method for manufacturing customized objects with controlled macro- and microporous structures.[33] In conventional tissue engineering approaches, the artificial matrices are fabricated first, followed by seeding of living cells, allowing them to attach, proliferate, and form new tissue. However, this method often leads to low initial cell density and inhomogeneous cell distribution, resulting in issues with tissue integration and implant rejection. An alternative approach utilizes so-called bioinks, made possible by advancements in 3D printing and ink formulations.[34] Bioinks allow for the fabrication of patient-specific tissues and organs with embedded living cells and bioactive compounds using a layer-by-layer (LbL) printing technique.[35,36] This approach enables precise control over the spatial arrangement of components and promotes homogeneous cell distribution.[37,38] Despite significant progress in 3D hydrogel bioprinting, challenges remain in term of optimizing the physical and biological characteristics of bioinks to enhance cell motility, proliferation, and differentiation.[39] The ultimate goal of bioprinting is to create 3D living scaffolds that mimic native human tissue. Achieving this would enable targeted repair, organ structure restoration, and reduced risk of implant rejection.[36]

However, bioprinting technologies encounter a challenging trade-off between printability, biocompatibility, and bioactivity. For instance, type 1 collagen is highly biocompatibility, but its limited self-assembly poses challenges for high-precision printing of cell-laden structures. Thus, recent studies have focused on modifying bioinks to improve printability and to enable bio-enhanced structures for tissue engineering and personalized regenerative medicine.[40,41]

Three main categories of bioprinting techniques exist: (1) material jetting, (2) vat polymerization-based bioprinting, and (3) material extrusion. Material jetting offers advantages,

such as low cost, high efficiency, high precision, and speed, allowing the precise deposition of materials and cells in non-contact and on-demand manner. Vat polymerization-based bioprinting provides exceptionally high resolution and precision, surpassing other technologies with printing resolutions of ~100 nm. Common challenges for both techniques include limited bioink viscosity, nozzle clogging, and a low achievable cell density ($\leq 1\times10^6$ cells mL^{-1}).[42] Moreover, material settling in the bioink reservoir can lead in cell density heterogeneity,[43,44] and the picolitre-range droplets in material jetting can be detrimental to cell viability after bioink deposition. Extrusion-based bioprinting, the most commonly used 3D printing technology, allows for high cell densities and the creation of heterogeneous models with precise cellular organization, crucial for artificial tissue and organ bioprinting. However, mammalian cell survival rates may be reduced to 40-85% due to the shear stress during the printing process.[42] We nevertheless chose extrusion bioprinting due to its widespread adoption in the field, and through systematic fine-tuning of the extrusion mechanism, nozzle diameter, control system, and hydrogel formulation. We have been able to successfully develop scaffolds with optimal printing resolution while preserving model fidelity and cell survival.

Inspired by the work of Biswas *et al.*,[45] who developed a GB-based hydrogel by incorporating phenyl boronic acid and achieved 98% cell viability of the entrapped cells, we aimed to optimize Guo-based hydrogels specifically for bioprinting applications. We first reported that large aromatic BA derivatives had an adverse impact on the hydrogels, while simple BA actually enhanced stability. However, we found that these hydrogels could only be functionalized with living cells after the printing process and were unsuitable as genuine bioinks.[17] In an alternative approach, we introduced polydopamine into GB hydrogels, effectively enhancing cell differentiation and

antibacterial properties. Nevertheless, similar to our previous formulation, only post-printing cell functionalization could be achieved.[16]

Here we report the development of a binary Guo-based hydrogel formulation capable of functioning as a true bioink, a significant advancement over our previous findings and a major breakthrough in the development of Guo-based hydrogels. We combined Guo and GMP with BA and K^+ ions. We hypothesized that a cross-association between Guo and GMP in the presence of K^+ and BA will further aid hydrogel formation and stability, and will allow for improved printability while ensuring cell survival and maintaining cell functionality. Specifically, we (i) identified and characterized a Guo and GMP hydrogel for wound healing purposes, (ii) encapsulated rMSCs in the Guo/GMP hydrogel, (iii) 3D bioprinted the mixture and characterized its properties, (iv) applied a biocompatible PEI coating[46] to minimize material spreading and serve as an interaction layer for proteins, dyes, and anti-tumor drugs,[47–49] and (v) evaluated both the absence of toxicity and the functionality of the entrapped cells.

2. EXPERIMENTAL SECTION

2.1. Materials. Guanosine (Guo), guanosine 5'-monophosphate (GMP) disodium salt, potassium chloride (KCl), boric acid (BA), phosphate buffered saline (PBS), hydrochloric acid (HCl), sodium hydroxide (NaOH), hyperbranched polyethylenimine (PEI), glutaraldehyde, paraformaldehyde (PFA), penicillin-streptomycin (Pen-Strep), fetal bovine serum (FBS), accutase cell detachment solution, hexamethyldisilazane (HDMS), fluorescein isothiocyanate-labeled dextran (FITC-dextran; average MW of 70, 500, and 2000 kDa, respectively), were all bought from Sigma-Aldrich (Saint Louis, MO, USA). Polylactic acid (PLA) was obtained from smartfilaments AG (Wil, Switzerland). Sterile syringe filters (polyethersulfone; PES), 0.2 μm, 25 mm), bovine serum albumin (BSA), Advanced DMEM (Dulbecco's Modified Eagle Medium),

glutaMAX, ReadyProbes™ Blue/Green Cell Viability Imaging Kit, CyQUANT™ lactate dehydrogenase (LDH) Cytotoxicity Assay, Na-azide (NaN$_3$), phycoerythrin (PE)-conjugated anti-rat CD90/mouse CD90.1 antibody, Alexa fluor 488 anti-mouse/rat CD29 antibody, Alexa fluor 488 anti-rat CD45 antibody, and PE-conjugated anti-CD34 antibody [ICO-115], and 7-AAD (7-amino-actinomycin D) Viability Staining Solution, were all obtained from Thermo Fisher Scientific (Waltham, MA, USA). StemXVivo® Adipogenic Supplement (100X) and Osteogenic/Adipogenic Base Media were both purchased from R&D systems (Minneapolis, MN, USA). All solutions were prepared using ultrapure Milli-Q water from a Gradient A 10 system (total organic carbon ≤4 ppb, resistance ≥18 MΩ cm; EMD Millipore, USA).

2.2. Guo and GMP ratio optimization and assessment of hydrogel formation. Guo and GMP were accurately weighed (see section 3.1 for details) into 2 mL reaction tubes (Eppendorf AG, Hamburg, Germany) along with 83 µL of KCl solution (300 mM), 83 µL of BA solution (300 mM), and the total volume was adjusted to 500 µL with Milli-Q water. The resulting solutions were heated to 80 °C and after approx. 5 min of stirring, the suspension became transparent. To induce hydrogel formation, the solutions were cooled to RT, and the grade of hydrogelation was evaluated by performing an inversion test as described previously.[16,17] Hydrogel imaging was done using a Nikon D3100 camera (Tokyo, Japan), and the hydrogel pH was determined using a pH meter (Mettler Toledo; Greifensee, Switzerland). To improve the hydrogel-forming characteristics, various concentrations of nucleosides, BA, and KCl were tested while keeping the Guo:GMP ratio constant at 1:1. Based on visual examinations after the hydrogels were cooled down to room temperature, samples demonstrating shape stability and no discharge upon inversion were classified as "gels". Compositions meeting this criterion were further assessed for printability.

2.3. Semi-quantification of printability. Guo/GMP hydrogels were prepared by accurately weighing the respective amounts of Guo and GMP in 16 mL glass vials, and adding KCl, BA, and Milli-Q water to 4 mL (all used weighs and volumes are described in section 3.2). Upon stirring and heating to 80 °C for approximately 15 minutes, the solutions turned clear. Next, the solutions were transferred into 3 mL syringes with parafilm-sealed tips and left undisturbed at RT to cool down gradually. After 1 h, the hydrogel samples were printed using a 20-gauge nozzle with an inner diameter of 0.58 mm using a Cellink BIO X[TM] bioprinter (Cellink, Gothenburg, Sweden). The printing settings were as follow: 37 °C for the nozzle, 25 °C for the substrate table, and a 2 mm s^{-1} printing speed. The perimeter of the printed squares, the area beneath free-floating printed filaments, and the area and angle of interconnected filaments (n=3) were all measured from images of the printed hydrogels using ImageJ[50] software (Figure 1). The printability of the bioinks was visually evaluated on the printed scaffolds, and compositions that yielded porous and layered structures were considered printable. The six layers of the printed hydrogels had an infill density of 15% and a scaffold area measuring 20 x 20 x 3 mm (length x width x height). Samples were labeled as X_Y, where X and Y represent the concentrations of Guo/GMP and BA/KCl (mM), respectively.

2.3.1. Filament collapse test. The filament fusion test was carried out as described elsewhere.[16,17,51–53] In brief, the CAD software SolidWorks (Dassault Systèmes, Waltham, MA, USA) was used to create a platform of seven pillars with preset spacings of 1, 2, 3, 4, 5 and 6 mm. A schematic of the 3D printed platform as well as an exemplary filament deposition is shown in Figure 1a. The platform was fabricated using a Ultimaker 2+ 3D printer (Utrecht, Netherlands), with PLA used as the scaffold material. The five pillars in the center and the corner pillars had dimensions of 2 x 10 x 6 mm^3 and 5 x 10 x 6 mm^3 (width x height x depth), respectively.

The collapse area factor C_f (as defined in equation 1) was calculated using the mid-span deflection of a dangling filament. Following the preparation of the appropriate hydrogel mixture, a single filament was placed on the platform, as illustrated in Figure 1a. The nozzle tip was positioned 0.3 mm above the pillar surface, and the print path was extended beyond the final pillar for 5 mm. One minute after filament suspension, a photograph of the deposited filament was captured and the area under the filament was measured using ImageJ.[50] As defined in equation 1,[51,53] C_f represents the percentage of deflected area after filament suspension (experimental area; A^c_e) versus the theorical area (A^c_t):

$$C_f = \frac{A^c_t - A^c_e}{A^c_t} \times 100 \qquad \text{Equation 1}$$

2.3.2. Filament fusion test. Under optimal gelation conditions, extruded hydrogel filaments exhibit a smooth surface and consistent breadth, resulting in uniform grids and square holes in the printed network. However, if the hydrogel is undergelated, the extruded filament may exhibit a partially liquid-like state, leading to fusions between upper and lower layers and resulting in the formation of more circular holes. For the filament fusion test (Figure 1b), a scaffold design was printed with an increasing filament-to-filament spacing of 1 to 5 mm in 1 mm intervals, and a photograph was taken 1 min after fabrication, as described previously.[16,17]

Three parameters were considered: (1) diffusion rate percentage (Df_r), which measures the extend of material spreading; (2) printability (P_r), which assess the shape of the printed grid holes; and (3) angular deviation rate (D_a), which indicates the degree of non-rectangularity. It is worth noting that ideal square shapes have a printability factor of close to 1, whereas small values for material spreading and angular deviation are desired. Angle deviation measurements were only performed for the 5x5 mm^2 square. These hydrogel characteristics were determined using the following equations, where A^f_t and A^f_e denote the theoretical and experimental pore areas,

respectively, L represents the pore perimeter, and θ_t and θ_e denote the theorical and experimentally measured grid angles:[51,52]

$$Df_r = \frac{A_t^f - A_e^f}{A_t^f} \times 100 \qquad \text{Equation 2}$$

$$P_r = \frac{L^2}{16A_e^f} \qquad \text{Equation 3}$$

$$D_a = \frac{\theta_t - \theta_e}{\theta_t} \times 100 \qquad \text{Equation 4}$$

2.3.3. Printability score. To determine optimal hydrogel compositions, individual scores were assigned to each sample based on their quality during the printability evaluation, following the methodology established in our previous studies.[16,17] Supplementary **Table S1** shows the scoring method for each of the tests.

In the filament collapse test, hydrogels with minimal filament bending (C_f value between 0 and 5%) were given a score of up to 40. Similarly, in the filament fusion test, all criteria were rated up to 40, and hydrogels with no material spreading (Dfr = 0) or perfect right angles (D_a are 0) received a score of 40 in both categories. For printability, the highest score was assigned to hydrogels with P_r values between 0.95 and 1, indicating grid holes with a perfectly square shape. The individual scores where then summed and normalized to a maximum possible score of 10, representing an overall printability index that can be used to compare different hydrogel formulations.

2.4. Preparation of PEI crosslinking of Guo/GMP hydrogel. To improve the properties of the printed hydrogels, three different Guo/GMP concentrations (90, 100, and 110 mM, with Guo:GMP at 1:1) were evaluated for PEI surface deposition, while KCl and BA were kept constant at 50 mM (as described in section 2.3). In brief, samples were immersed in a PEI solution (5 mg mL^{-1}) for 15 minutes within a humidified incubator at 37 °C with 5% (v/v) CO_2, after which the PEI solution was removed, and the hydrogels were gently washed with PBS three times. The hydrogel was then

incubated in fresh Advanced DMEM complete media at 37 °C for up to 7 days in the same humidified incubator. The medium was replaced every 2 days, and hydrogel stability was monitored by capturing photographs of the printed scaffold and measuring the area of the scaffold pores using ImageJ.[50]

2.5. Rheological studies. For rheological studies, a Guo/GMP hydrogel solution was prepared by combining Guo, GMP, KCl and BA (100 mM, 100 mM, 50 mM, 50 mM respectively), and heating the mixture with stirring to 80°C for 15 min. For sample preparation, PLA molds with a diameter of 20 mm were created using SolidWorks and 3D-printed with a Sigma R19 printer from BCN3D Technologies (Gavà, Barcelona). Then, Guo/GMP hydrogel solutions (2 mL) were transferred into the PLA molds and left undisturbed at RT. After 1h, the samples were gently transferred into a solution of PEI (5 mg mL^{-1}) and incubated at 37 °C within a humidified incubator (5% (v/v) CO$_2$) for 15 minutes. After incubation, the PEI solution was removed and the hydrogels were washed three times with PBS. Finally, the rheological characteristics were evaluated using a Discovery HR-2 hybrid rheometer from TA Instruments (New Castle, DE, USA).

Six distinct experiments using two different Peltier geometries were carried out: (i) a strain sweep and (ii) an oscillating stress scanning experiment, both with a parallel stainless steel 20 mm diameter Peltier plate; (iii) a dynamic step-strain sweep using a cross-hatched 20 mm diameter Peltier plate; (iv) a peak-hold assay with the same Peltier set-up; (v) a viscosity and (vi) compression test, both performed with a parallel stainless steel Peltier plate. The strain sweep experiment was carried out using a 1 Hz oscillation frequency and testing a strain range from 0.01 to 100%. In the oscillating stress scanning experiment, a shear stress ranging from 0.01 to 300 Pa was applied at an angular frequency of 10 rad s^{-1} with a linear increase and decrease pattern to generate a hysteresis loop. The process was repeated until three complete loops were recorded for

each experimental condition. For the dynamic strain sweep experiment, a strain ranging from 0.1 to 100% was used over 100 s and 10 cycles at a constant rotational frequency of 10 rad s^{-1}, while during the peak-hold test, the sample was subjected to a 10 s phase with a shear rate of 3.45 s^{-1}, followed by a 60 s recovery phase with a shear rate of 0.1 s^{-1}. The recorded storage modulus (G') and the loss modulus (G'') were used to evaluate the elastic properties and fluidity in the different setups such as the strain sweep, dynamic step-strain sweep, and peak hold assay. Finally, the axial compression test was performed using a constant speed of 100 μm s^{-1} over 46 s. All experiments were carried out at 37 ˚C and repeated at least 5 times for each sample.

2.6. Morphological analysis of the Guo/GMP-PEI hydrogels. Samples described in section 2.5 were submerged in a fixative solution of glutaraldehyde (1.0% (w/v) in PBS) for 1 h at RT. Then, samples were rinsed 3x with PBS and dehydrated using a series of ethanol washes consisting of 25%, 50%, 70%, 85% (3x), 95% (3x), and 100% (3x). Next, the samples were submerged in HDMS for 10 min and vacuum dried at RT. Finally, samples were coated with gold using a Sputter Coater AGB7340 (Agar Scientific, Stansted, UK) and evaluated using a Zeiss Merlin field emission scanning electron microscope (FE-SEM; Carl Zeiss NTS GmbH, Germany). Five photos were acquired for each sample at different Z-levels using a working distance of 5 mm and a potential of 2 kV.

To assess the permeability of the Guo/GMP-PEI hydrogel for nutrients and small molecules, three FITC-dextran variants with MWs of 70, 500, and 2000 kDa were employed.[54] Guo/GMP-PEI scaffolds were directly printed into 6-well plates, loaded with 4 mL of the respective FITC-Dextran solution at 1 mg mL^{-1} in medium, and the loaded scaffolds were then incubated at 37 °C for 10 h. The incubation solution was carefully removed and the remaining fluorescence intensity (ex = 450 nm, em = 550 nm) of the solution was measured using an Infinite M Nano multimode

plate reader (TECAN, Switzerland) after transferring 100 µL into a 96-well microplate. After rinsing the hydrogels 3x with PBS to remove any non-internalized FITC-dextran, the hydrogels were incubated with fresh media for an additional 10 h, and the intensity of the supernatants was measured as described above. This procedure was repeated three times, with triplicates taken for each FITC-dextran solution and incubation time.

2.7. Cell Experiments. *27.1. rMSC isolation and culture.* Male Sprague-Dawley rats aged five weeks were euthanized using CO_2 inhalation and femoral bones and tibia were isolated from the hind legs by removing muscles and connective tissues. Bone marrow cells were collected, filtered through a 40 µm cell strainer, and centrifuged at 200 rcf for 3 min in Advanced DMEM medium. For cell culture, T75 flasks were used to plate 1500 cells per square centimeter in Advanced DMEM medium containing both sodium pyruvate (0.11 g L^{-1}) and glucose (4.5 g L^{-1}), and supplemented with 1% (v/v) GlutaMAX, 20% (v/v) FBS, and 1% (v/v) Pen-Strep solution (10 000 U mL^{-1} penicillin G and 10 mg mL^{-1} streptomycin).

All animal experiments were conducted in strict accordance with the guidelines of the EU Directive 2010/63/EU, the Spanish Royal and Catalan Decrees 1201/05 and 214/97, respectively, and the Catalan Law 5/95. The study was approved by the Institutional Ethics Committee on Animal Experimentation (Comitè d'Ètica en Experimentació Animal) of the Autonomous University of Barcelona (UAB), which provided the euthanized rats for our research (procedure ref. 10906 from the Generalitat de Catalunya).

To confirm rMSC cell authenticity, surface markers were analyzed using flow cytometry. Cells were harvested by centrifugation, the supernatant discarded, and the individual cell pellets resuspended in basic flow cytometry buffer consisting of PBS, 1% (w/v) BSA, 2 mM EDTA, 0.1% (w/v) sodium azide). Cell densities were adjusted to 5×10^5 cells mL^{-1}, re-pelleted (5 min, 1500

rpm), and resuspended in 100 µL of blocking buffer (PBS supplemented with 3% (w/v) BSA and 0.1% (w/v) sodium azide). After incubation for 30 min at RT, cells were re-pelleted, and 100 µL of the corresponding antibody solutions (anti-rat CD90/mouse CD90.1, anti-mouse/rat CD29, anti-rat CD45, and Anti-CD34) were added and samples incubated in the dark at 4 ºC. After 20 min of incubation, 1 mL of basic flow cytometry buffer was added, and samples subjected to centrifugation at 1500 rpm for 5 min. Cells were resuspended in 1 mL of blocking buffer, and 5 µL of 7-ADD solution were added. Single-cell suspensions were formulated, and samples analyzed using a Beckham Gallios Flow Cytometer (Boston, MA, USA).

Importantly, only cells between passage two and five were used for subsequent cell experiments, and cell media (complete Advanced DMEM) was exchanged every 2 days. Subconfluent cells were harvested by adding 4 mL of Accutase solution. After 5 min of incubation, the cell suspension was aspirated, pelleted, and resuspended in complete cell media. All cell-based tests were performed as 3 separate biological replicates, with each replicate consisting of 3 technical duplicates.

2.7.2. rMSC-laden Guo/GMP-PEI hydrogels. Guo and GMP were sterilized using UV light for 20 min, whereas the BA and KCl solutions were sterile filtered using 0.2 µm PES syringe filters. Guo/GMP hydrogel solutions were then prepared as stated above (section 2.3) under sterile circumstances and allowed to cool down to 37 °C in 3 mL syringes. To entrap the cells homogenously within the Guo/GMP hydrogels, 750 µL of the cooled gel were transferred into a new syringe, followed by 50 µL cell suspension (10^6 cells in 200 µL complete medium, RT), and repeating the procedure two times. After adding a final layer of 750 µL Guo/GMP hydrogel, the layers were mixed by passing the content gently between two syringes at 37 °C. Up to 6 scaffold

layers were printed, each with dimensions of 20 x 20 x 3 mm (L x W x H) and an infill density of 15% (as detailed in section 2.3), and subsequently coated with PEI, as described in section 2.4.

2.7.3. Cell proliferation and viability experiment. To assess cell proliferation and viability, we measured LDH activity in the cell medium after induced cell lysis. In brief, rMSC-laden Guo/GMP-PEI hydrogels were immersed in complete medium for 1, 7, 14, and 21 days at 37 °C and 5% CO_2. After each incubation period, the cell media was carefully aspirated, the hydrogel scaffolds washed three times with PBS, and the samples treated with 200 µL of 0.2% Triton X-100 in PBS to induce cell lysis and degrade hydrogel scaffolds. Then, 50 µL of the conditioned cell culture medium were added to 50 µL of assay reagent in a 96-well plate, incubated in the dark for 30 min, and absorbance was measured at 490 and 680 nm with an Infinite M Nano microplate reader.

2.7.4. Cell distribution in the Guo/GMP-PEI hydrogels. Prior to entrapping the rMSCs in the Guo/GMP-PEI hydrogel, the adherent cells were stained with Deep Red CellTracker™ solution (5 µM in serum free media) and incubated for 30 min at 37 °C according to the manufacturer's protocol. Stained rMSCs were then entrapped in the Guo/GMP-PEI hydrogel as described above (see section 2.7.2). After 3D bioprinting (10 x 10 mm scaffold and 2 layers) and PEI treatment, the fluorescence of the embedded cells was monitored using a confocal laser scanning microscope (CLSM; Leica Microsystems GmbH) using a 5x objective, excitation/emission wavelengths of 630/660 nm, respectively, and an argon laser. The entire scaffold surface was analyzed, and a z-stack of 30 images recorded. All images were processed using the Imaris Image Analysis Software (Oxford Instruments).

2.7.5. Cell morphology. rMSC-Guo/GMP-PEI hydrogels were incubated at 37 °C and 5% CO_2 in complete medium. Controls included cells alone and unloaded Guo/GMP-PEI hydrogels. After

different incubation times, the cell-laden hydrogels were rinsed two times with PBS to remove loosely adherent cells. The hydrogels were then fixed for 30 min in 4% PFA (in PBS) and washed three times in PBS. To decrease non-specific dye binding, the cells were permeabilized using Triton X-100 (0.1% in PBS) for 20 min at RT, followed by a 1 h soak of the hydrogels in a solution of BSA (10 mg mL^{-1} in PBS). rMSC-Guo/GMP-PEI hydrogels were then stained with 0.1 µg mL^{-1} Alexa Fluor 488 phalloidin (in PBS) for 1 h in the dark, and following 3 washes with PBS, hydrogels were incubated for 5 min in the dark and RT in a 20 µg mL^{-1} DAPI solution (in PBS). After 3 further PBS washes, hydrogels were photographed using a LEICA Microsystems CLSM with a 63x oil immersion objective and excitation/emission wavelengths of 405/440-480 and 488/495-545 for DAPI and phalloidin-Atto 488 detection, respectively.

2.7.6. Cell functionality and adipogenic differentiation. In order to assess the functionality of the entrapped cells in the Guo/GMP-PEI hydrogel, their adipogenic development was evaluated. In brief, 3D bioprinted cell-laden hydrogels were incubated for up to 21 days, first in complete medium for one day, then in osteogenic/adipogenic base media with adipogenic supplement (adipogenic induction medium). As controls, non-cell laden printed hydrogels and cells seeded on a cover glass were used under the same conditions. Negative controls included cell-laden scaffolds cultured in basal medium. At different time points, samples were analyzed for adipogenic differentiation by lipid droplet staining using Oil red O staining solution (Sigma-Aldrich, Saint Louis, MO, USA). In brief, the rMSC-Guo/GMP-PEI hydrogels were first fixed using 4% PFA for 30 min. Then, the hydrogel scaffolds were washed two times in PBS and incubated with Oil red O solution (mixed 3:2 in water) for 30 min. Hydrogels were then washed again in PBS for two times, and stained hydrogels were imaged with a CLSM using excitation/emission wavelengths of 552/615-630 nm.

2.8. Statistical Analysis. All data were analyzed in SPSS software (IBM, Armonk, NY, USA) using one-way ANOVA with a confidence level of 95% ($\alpha = 0.05$) followed by multiple comparison correlation and Tukey's post hoc test (*$p \leq 0.05$, **$p \leq 0.01$, ***$p \leq 0.001$ and ****$p \leq 0.0001$).

3. RESULTS AND DISCUSSION

Many recent studies in tissue engineering have focused on the development of bioinks using Guo-derivatives[11,14,55] due to (i) their dynamic nature which enables them to regain their properties after damage; (ii) their capacity to retain a high amount of water; and (iii) their highly-suitable microenvironments for cell survival. In this project, we explored the potential of novel binary Guo/GMP hydrogels as bioinks, and in particular, the use of a PEI coating to further improve their physicochemical properties. Importantly, while Guo represents a rather insoluble nucleoside capable of hydrogel formation even at low concentrations, GMP requires high concentrations due to its high solubility at neutral pH. Thus, when combined, GMP is suggested to enhance Guo solubility through intermolecular interactions, whereas Guo, in turn, facilitates GMP gelation already at lower nucleoside concentrations. Hence, we focused on binary Guo/GMP hydrogels and tested various compound ratios in combination with KCl and BA to optimize hydrogel printability and, most importantly, cell viability and proliferation. However, due to material spreading, the tested Guo/GMP hydrogels were unable to preserve their shape and porosity after 3D printing. To overcome this problem, we developed a PEI surface coating to increase long-term shape stability.

3.1. Guo and GMP ratio optimization and assessment of hydrogel formation. In a first step, we aimed to establish the most favorable Guo and GMP ratio (Figure 2a) that, when combined with BA and KCl at constant concentrations, would produce a hydrogel at physiological pH.[14,56–58] Notably, neither the absence of Guo nor the presence of low Guo concentrations in GMP solutions (ratio Guo:GMP 0:1 and 1:4) led to gelation, regardless of the tested nucleoside concentrations. In contrast, gel formation was observed when the Guo:GMP ratio was increased, which might be attributed to the reduction of repulsive forces between the anionic GMP molecules through the incorporation of Guo. Moreover, to ensure optimal conditions for cell viability and to

minimize cell death, we aimed for a near-neutral pH. Notably, the obtained gels showed a basic pH when little to no amounts of Guo were added (ratio Guo:GMP 0:1 and 1:4), while the pH was acidic for compositions with Guo:GMP ratios of 2:1, 4:1 and 1:0. In our set-up, only a 1:1 Guo:GMP ratio resulted in a pH suitable for bioinks, and thus, all subsequent experiments were performed with this ratio while varying the concentrations of the components.

To further optimize the Guo/GMP hydrogel compositions, we then evaluated gel appearance as either opalescent (i.e., some Guo is still undissolved and crystallin) or transparent (i.e., all Guo was dissolved and gelated homogenously), and assessed flow stability by inversion test (Figure 2b). Various concentrations of BA and KCl were combined with different Guo/GMP concentrations while maintaining their 1:1 ratio. Notably, transparent and homogeneous gels were obtained in a wide range of combinations (Figure 2bi), suggesting homogenous distribution off all components throughout the hydrogel network. However, when the Guo concentration exceeded 110 mM, white and opalescent gels were observed, probably due to partial Guo precipitation and indicative of incomplete incorporation of the nucleoside into the internal hydrogel structure.

3.2. Semi-quantification of printability. 3D printing enables the formation of predefined structures by LbL assembly. Several advantages of 3D printing for biomaterials have been reported, such as the capacity to form complex and patient-customized shapes.[59] We first assessed printability of the newly developed bioinks by visual inspection of the printed structures (Figure 3a) and designated hydrogels as printable when they exhibited porosity and distinct layers. Such qualitative inspections enable a rapid assessment of the relative shape fidelity among different hydrogel formulations and aids the identification of favorable and unfavorable parameters for 3D printing. However, it may not facilitate direct comparisons between hydrogels derived from very distant compositions.

Even though there were clear visual differences between low and high Guo compositions, they were rather subtle within the range of 80 to 100 mM. As expected, sample viscosity increased with higher nucleoside concentrations, resulting in printable hydrogels when using 80 mM or higher concentrations of each nucleoside, and crucially, without causing nozzle jam. In undergelation conditions (i.e., too low nucleoside or too low BA/KCl concentrations), the printed hydrogels fused at the cross sections, while for overgelated conditions, a fractured morphology and irregular filaments were observed (see Figure 3b for representative images of both printable and no printable hydrogels). However, for optimal hydrogel compositions, smooth and uniform filaments were continuously extruded, resulting in grid patterns with well-defined square pores. Importantly, all developed hydrogels displayed a neutral pH of 7.0 ± 0.3. This was attributed to the 1:1 ratio of Guo:GMP which consistently resulted in a pH of 7.0 ± 0.08. Consequently, this ratio was kept unaltered in order to ensure that all printable hydrogel formulations would be suitable as bioinks.

After identifying printable formulations (from 80 to 110 mM for Guo and GMP, and from 30 to 60 mM for BA and KCl), we next sought to identify optimal compositions for 3D printing. To achieve a comprehensive assessment and scoring of our hydrogels, two distinct tests and five property parameters were evaluated.[51,52,60] Schematics of the used platform and the printing pattern are depicted in Figure 1, while the experimental results are summarized in Figure 4.

The qualitative assessment of the collapse test for different compositions of Guo/GMP hydrogels (Figure 4ai) demonstrated that no filament collapse was observed after one minute, and that only minor deformations were detectable after 12 h (data not shown). Importantly, such slow deformations are neglectable as printing timeframes are typically in the order of minutes, and as we planned to utilize a post-printing treatment to further enhance hydrogel stability.[39] Intriguingly, the C_f rose with increasing Guo/GMP concentrations, however, the changes were statistically not

significant. This trend could be attributed to the increased density and weight of the respective hydrogels, potentially causing simply due to gravity.

To assess filament fusion and pore closure for each hydrogel composition, their respective D_{fr}, P_r and D_a were determined (Figure 4aii, aiii and aiv). To ensure minimal impact of the plastic-hydrogel interaction and obtain unaltered results for the bioink, two layers of the hydrogel pattern were printed, and only the upper layer was analyzed. When the capillary forces exceed the yield strength of the printed soft material, pore closures occur as a result of increased corner deformation.[51] Notably, no significant differences were observed in diffusion rate and printability between the tested gel compositions and their pore closure characteristics. Moreover, there were no instances of filament distortion or fracture during the printing process, indicating optimal hydrogel viscosity.[61] However, pores with smaller sizes, specifically 1x1 and 2x2 mm, were exclusively prone to closure. This may be attributed to the rather wide nozzle size (0.58 mm), as even minor filament spreading can lead to pore closure in this setting.

Robust and reliable angle printing represents a key property of bioinks as it assesses the bioink behavior when the printing direction has to change abruptly. For this, we assessed the top right square of each printed pattern by joining the center points of each corner and calculating the enclosed angle (Figure 1). While Guo concentrations of 90, 100, and 110 mM performed best, the angle deviation rates of all tested bioinks were lower than 16%.

To enable a reproducible and sensible comparison of our hydrogel formulations, we established a normalized scoring scheme for each of the tested parameter (as detailed in section 2.3.3).[16,17] As summarized in Figure 4b as scores ranging from 1 to 10, bioinks 90_50, 100_50 and 110_50 exhibited the best overall performance for printability and shape fidelity. Importantly, such a scoring methodology provides critical semi-quantitative insights into the printability

characteristics of the hydrogels that cannot be obtained solely through visual inspection of the extruded filament or the printed structure.[62,63] Furthermore, the obtained scores are highly objective, enabling a reliable comparison of bioinks with different compositions. However, highly for divergent bioink families, additional parameters may be necessary to effectively utilize such a scoring system.

3.3. Guo/GMP-PEI hydrogel preparation and characterization. To enhance the long-term stability of the 3D printed hydrogels, a layer of PEI was applied onto Guo/GMP hydrogels. PEI is a hydrophilic macromolecule that contains primary, secondary, and tertiary amine groups, and its hyperbranched structure provides large polar contact areas, enabling interactions with other biomaterials. For instance, Yildirimkaraman *et al*.[64] developed an electroactive nanogel coating using the LbL technique consisting of branched PEI and alkyne containing polyester on a gold surface. We hypothesized that the hyperbranched PEI structure would facilitate the formation of a 3D hydrogen bonding network between the -NH$_2$ groups of the PEI compound and the phosphate group of the GMP, while preserving the integrity of the scaffold (Scheme 2).[65]

The Guo/GMP hydrogels (90_50, 100_50 and 110_50) were immersed in PEI solutions at concentrations of 0.5, 1.0, 5.0, and 10 mg mL^{-1} for 5, 15, 30, and 60 min (Figure S1, Supporting Information). After evaluating the normalized area of the scaffoldd, no further improvement was achieved beyond a PEI concentration of 5 mg mL^{-1} and a 15 minutes incubation time. Therefore, these settings were selected in subsequent experiments.

The deposition of PEI onto the hydrogels was verified by observing an increased integrity of the hydrogel network after 24 h of incubation at RT (Figure 5a). To further examine hydrogel stability, the coated scaffolds were incubated in Advanced DMEM medium at 37 °C for a duration of up to 7 days, and the scaffolds and pore area were assessed every 24 h using ImageJ[50] (Figure 5b).

Notably, only a small reduction in the normalized scaffold area was observed over time, and no significant differences were detected among the three tested compositions. Using the 100_50 composition, we then evaluated the development of the pore area over time (Figure 5c); after an initial ~25% decrease within the first 24 h, the pore area stabilized and did not decrease significantly decrease beyond day 3.

To investigate the mechanical properties of the Guo/GMP-PEI hydrogels, rheological measurements were performed. Both the elastic properties and fluidity were measured by G' and G'', which were monitored under various condition, including strain sweep, dynamic step-strain sweep, and peak hold assay. The elastic nature of the sample was determined by strain amplitudes ranging from 0.01 to 100% at an oscillation frequency of 1 Hz (Figure 6a). With increasing strain, G' exceeded G'' until reaching a strain of 6.93 percent, where a turning point was observed, and the reverse trend was detected as the strain was further increased. This behavior could potentially be attributed to the breakdown of intermolecular or π- π stacking interactions. Thus, to ensure the hydrogel maintained its elastic nature, a strain of 0.1% was selected for subsequent experiments.

We then performed a recovery test to study the self-healing capabilities and recovery time of the Guo/GMP-PEI hydrogels. First, the strain was held at 0.1% for 100 s. Then, the strain was increased to its maximum value of 100% and held for an additional 100 s, after which the effect was evaluated (Figure 6b). This procedure was repeated for a total of 5 shear/recovery cycles. Importantly, while the hydrogel retained its elastic behavior (G'>G'') when subjected to a constant strain of 0.1%, its viscoelastic properties were lost with a strain of 100% (G'<G''). However, upon reducing the strain back to 0.1%, the broken hydrogel returned to its initial state within a few seconds in all 5 cycles and recovered ~90% of its original viscosity. Moreover, after a 100 s recovery period at a strain of 0.1%, the initial viscosity was fully recovered. This self-healing

capacity can be attributed to the dynamic noncovalent interaction network present in the hydrogel (e.g., hydrogen bonds, ionic interactions, or π-π stacking), which can reform after experiencing stress and thus reestablish hydrogel stability. Due to this thixotropic behavior, Guo/GMP-PEI hydrogels may represent easily injectable soft hydrogels.

Figure 6c shows the "peak-hold" experiment, in which the hydrogel is subjected to a short shearing stress followed by a defined recovery period, while monitoring the viscosity response. First, an initial shear rate of 3.45 s^{-1}, corresponding to the shear rate used during the 3D printing of the hydrogel, is applied. After ~5 s, the viscosity stabilizes, and after 10 more seconds, the shear rate is reduced to 0.1 s^{-1}. Following an initial overshoot, which may be attributed to a flow instability and polymer desintanglement,[66] the viscosity of the system stabilized after ~10 s under low shear stress. Importantly, when a second layer of hydrogel was applied, a stable viscosity was observed, indicating that the filaments maintained their stability without merging.

Figure 6d shows the hysteresis loop curves of the hydrogel at 37 °C and a shear stress change from 0.01 to 300 Pa. In the beginning, a low shear stress is applied to produce strain in the system. As the strain accumulation reaches the yield strain, the hydrogel structure begins to crack and flow, rapidly increasing the shear rate. The shear rate and stress then gradually increase, but not uniformly. However, while the shear rate does not increase uniformly due to the simultaneous decrease in viscosity, the shear stress increases abruptly due to structural cracking.[67] As the shear stress decreases, the viscosity gradually increases and the hydrogel's structure is recovered. The rapid decrease in the shear rate observed the fast recovery of the Guo/GMP-PEI hydrogel. Additionally, the hydrogel exhibited on-time recovery, meaning that the upward and downward curves coincide and do not deviate from the shear stress axis, and the area of the hysteresis loop reflects the thixotropy of the system.[67] Importantly, hysteresis loops, the recorded area remained

constant for all three loops, indicating that the gel structure remained undamaged and demonstrating the hydrogel's fast recovery rate. These results confirmed the self-healing capabilities of Guo/GMP-PEI hydrogels found in our other rheology experiments, and corroborated the hydrogel's injectability and printability. Moreover, shear-thinning behavior is an important criterion for hydrogel injectability. This decrease in viscosity upon stress allows the hydrogel to restore its network of reversible interactions and thus regain its original properties. As evident from the flow experiment (Figure 6e), the viscosity of the developed Guo/GMP-PEI hydrogel decreases significantly for shear rates larger than 10^{-2} s^{-1}, demonstrating its shear-thinning capacity. Next, an axial compression test was performed to evaluate the general toughness and strength of the hydrogel and to determine the elastic modulus (Figure 6f). We observed that the compressive strength of the Guo/GMP-PEI increased until reaching a strain of ~20%, after which it stabilized until ~25%, where it exhibited a compressive strength of 0.6 MPa and an elastic modulus of 0.037 MPa.

The macroscopic morphology of the hydrogels was further examined using SEM. The SEM images of the Guo/GMP-PEI hydrogel clearly revealed the presence of a dense and nanofibrillar 3D network within the hydrogel (Figure 7ai). Additionally, our analysis revealed a significant number of nanofibers of Guo/GMP in the range of ~24-31 nm (25.5 ± 0.6 nm, Figure 7aii), which play a crucial role not only for hydrogel formation but also in its stabilization.

Based on these results, we then used the developed Guo/GMP-PEI hydrogel formulation to print a larger and more complex 3D structure. First, a jar was designed in SolidWorks software (Dassault Systèmes, Vélizy-Villacoublay, France) (Figures 7bi) and subsequently printed (Figures 7bii and 7biii). The printed hydrogel jar demonstrated good stability even 2 h after printing, showing no

signs of collapse or deformation. Furthermore, when water was added, the jar maintained its shape and retained its contents despite the additional forces exerted by the liquid.

3.4. Permeability. To examine the uptake, release, and diffusion of nutrients within the hydrogel matrix, a series of *in vitro* studies was performed. First, the printed Guo/GMP-PEI hydrogels (1.5 mL of hydrogel) were immersed in solutions of FITC-Dextran with specific molecular weights (70, 500 and 200 kDa; 1 mg/ml) at 37 °C. After 10 h, an aliquot (100 µL) was removed from the supernatant, and the fluorescence intensity was measured (see Supporting Info, Figure S2). The decrease in fluorescence intensity observed in the surrounding solution is attributed to the FITC-Dextran uptake into the hydrogel matrix. The hydrogel was then washed three times using PBS to remove excess FITC-Dextran, immersed in medium for another 10 h at 37 °C, and the fluorescence intensity of the solution measured. This process was repeated three times to monitor the release of FITC-Dextran. This demonstrated that after 10 h of immersion, ~80% of the FITC-Dextran molecules had diffused into the 1.5 mL hydrogel, independent of their molecular weight (Figure 8). Moreover, after transferring the FITC-dextran loaded hydrogels into medium, approx. the same timeframe was required to ensure an ~100% release from the gel matrix. Importantly, Axpe *et al*.[68] established the significance of solute and mesh size for molecular transport, and for our PEI-coated hydrogels, all tested FITC-Dextran molecules diffused freely through the matrix, and increasing the molecular weight did not lead to reduced diffusivity. Hence, it is reasonable to infer that the various nutrients present in the surrounding media or environment will also be capable of being taken up and released by the hydrogel, with likely constant diffusion rates in both directions. These properties are of paramount importance for applications involving cell-entrapped hydrogels.

3.5. Cell experiments. To incorporate rMSCs into the Guo/GMP hydrogels, distinct bilayers of gels (750 µL) and rMSCs solution (50 µL) were passed back and forth 6 times between two

syringes at 37 °C (Figure S3, Supporting Information), 3D printed, and coated in a solution of PEI (5 mg mL^{-1}; 15 min, 37 °C).

3.5.1. Cell experiments. To evaluate the biocompatibility of the rMSC-Guo/GMP-PEI hydrogel, we monitored cell proliferation and viability using the LDH assay. rMSCs were incorporated into Guo/GMP-PEI hydrogels and the cells monitored for up to 21 days. As shown in Figure 9ai, the quantity of rMSCs showed a consistent increase throughout the monitoring period, albeit at a slightly slower rate on days 7 and 14 when compared to cells seeded on tissue culture polystyrene (TCPs) plates. However, after 21 days, no significant difference was observable. Additionally, cell viability readings were compared to those from cells cultured on TCPs plates. While cell survival was ~90% on days 1, 7, and 14 for the Guo/GMP-PEI hydrogel, it increased to approximately 100% on day 21 (Figure 9aii). These results align with previous studies that have demonstrated the capacity of Guo to support cell growth and survival.[69,70] Importantly, these results demonstrate that neither the Guo/GMP-PEI hydrogels nor the 3D printing procedure resulted in cytotoxic effects on the embedded rMSCs. Additionally, the effectiveness of the PEI coating on Guo/GMP hydrogels was further demonstrated through a scaffold area study (Figure 9b). Whereas non-treated Guo/GMP hydrogels completely dissolved in complete medium within 3 days, PEI-treated hydrogels showed only a 10% decrease in hydrogel area after 4 days and remained stable thereafter.

A commonly encountered issue when using cell-entrapped hydrogels is uneven cell density or cell type distribution throughout the scaffold core, typically caused by incomplete mixing of the hydrogel and cell solution prior to printing.[71]. Thus, we analyzed not only rMSCs on the surface but also within the printed scaffold by doing z-projections. As depicted in Figure 10a, a homogenous cell distribution along the printed hydrogel surface and within the scaffold core was

observed, confirming effective mixing and homogenous cell distribution (Figure S3). Next, the cell morphology of the embedded rMSCs was evaluated by staining the actin filaments and nuclei followed by CLSM. Cell imaging revealed a roundish morphology even after 21 days of incubation for both rMSCs-entrapped in the Guo/GMP-PEI hydrogel and those seeded onto a 2D Guo/GMP-PEI hydrogel (10 x 3 mm, width x height). In contrast, control cells seeded on a cover glass displayed a spread morphology with a well-defined cytoskeleton (Figure 10b; please refer to Figure S4a for additional time points). Thus, both the 2D and 3D systems resulted in a roundish cell morphology and a cluster-like organization, similar to what has been described for alginate-based systems.[72,73] However, after 3 days of incubation, the cells started to show a stellate morphology, accompanied by the emergence of actin-rich protrusions known as invadopodia (Figure 10a and b, red arrows; refer to Figure S4a and b for additional time points). And moreover, we were able to demonstrate adipogenic differentiation and thus functionality of the embedded rMSCs by monitoring the formation of lipid droplets (LDs) by Oil-red O staining at different time points (Figures 10c and S4c). Importantly, the presence of LDs indicates the development of specialized energy storage organelles within adipocytes.[74,75] Based on our results, the entrapped rMSCs underwent differentiation towards an adipogenic linage around day 7, when first lipid droplets could be identified, and which increased in numbers over subsequent days.

4. CONCLUSIONS.

The development of versatile bioinks that mimic soft tissues is of utmost importance for the production of customized scaffolds to facilitate tissue repair and replacement of damaged or missing tissues. Supramolecular hydrogels, especially nucleoside-based hydrogels, have garnered growing interest in tissue scaffolding applications owing to their excellent biocompatibility. Unlike previous studies where guanosine-based hydrogels faced limitations in terms of printability

and cell viability, our binary hydrogel system shows significant potential as bioink due to its ability to encapsulate living cells, maintain their viability, and be compatible with 3D printing.

In this study, we describe a comprehensive workflow for creating a bioprintable binary hydrogel containing entrapped rMSCs, followed by a thorough characterization using diverse physicochemical approaches. For example, SEM analysis confirmed the formation of an extensive nanofibrillar network within the hydrogel matrix, and the applied PEI coating ensured hydrogel stability in medium for ≥21 days. Moreover, even after 21 days of incubation, the embedded cells showed a high cell viability of 85%, which is crucial for effective scaffold biointegration. Additionally, the rMSCs were evenly distributed throughout the printed Guo/GMP-PEI hydrogel. Although the cells maintained a rounded morphology (i.e., undifferentiated) at various time points, the presence of lipid droplet was observed after 7 days under adipogenic conditions, demonstrating successful differentiation and functionality of the encapsulated cells.

In summary, our study demonstrates the significant potential of Guo/GMP-PEI hydrogels as biomimetic materials for soft tissue reconstruction, which can be further customized by incorporating additional biomolecules to improve cell differentiation or elicit specific cellular responses.
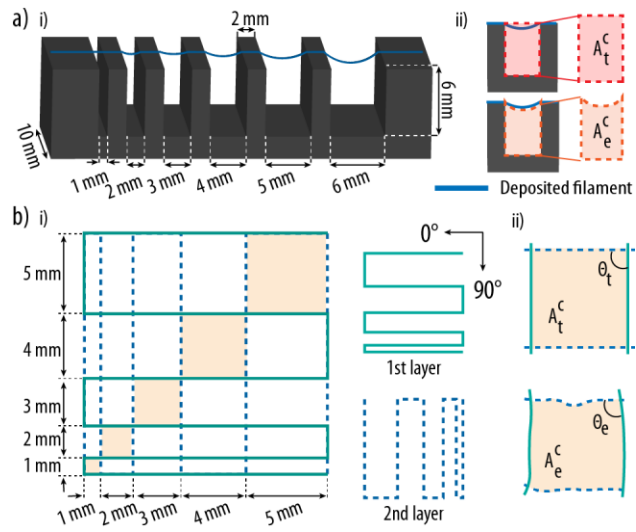
Figure 1. Bioink printability assessment. a) Analyzed as side views (i) three-dimensional (3D) printed platform was utilized to determine the filament collapse area; (ii) representation of the theorical (up) and experimental (bottom) region under the printed filament. b) (i) Fusion test printing pattern consisting of two filament layers deposited at 0° and 90°; (ii) theoretical (top) and experimental (bottom) regions are represented. Top views were analyzed. Adapted with permission from reference 14. Copyright 2023 MDPI.
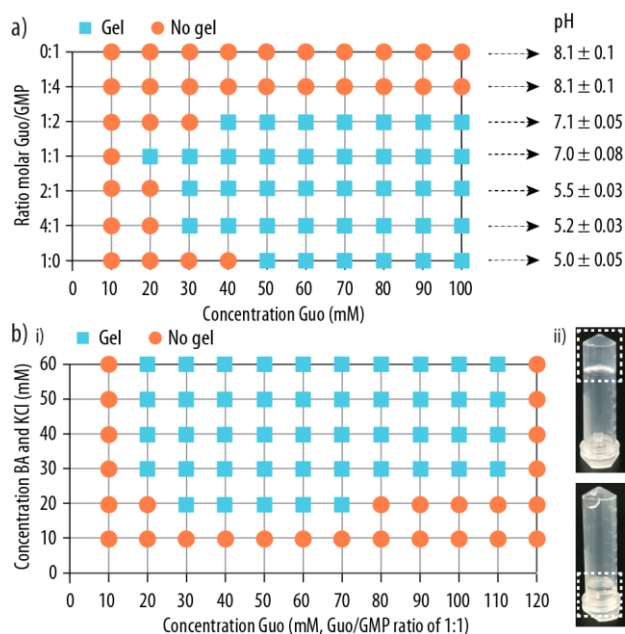
Figure 2. Gelation assessment of binary guanosine and guanosine 5'-monophosphate (Guo/GMP) hydrogel using a vial inversion test. a) Classification of the binary solutions as gelated (gel; blue square) and non-gelated (no gel; red circle) as a function of Guo and GMP ratios and nucleoside concentrations after 1 h cooling down at room temperature (RT). The concentrations of boric acid (BA) and potassium chloride (KCl) were kept constant at 50 mM, and the pH of the obtained Guo/GMP solutions is indicated on the right. b) (i) Phase diagram of binary hydrogel gelation as a function of nucleoside (x-axis) and BA/KCl concentration (y-axis) after 1 h of gelation at RT. (ii) Images of binary solutions classified as gelated (up) and non-gelated (down) are shown and their positions after tube inversion are shown by a dashed white box.
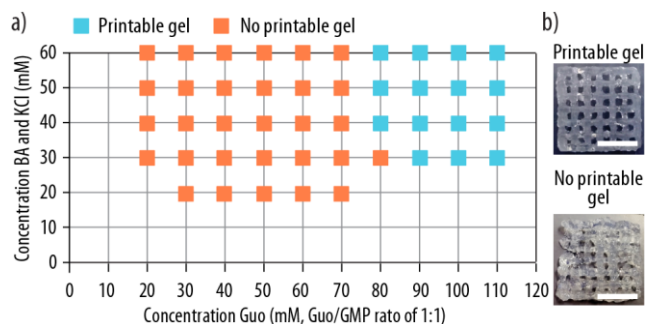
Figure 3. Printability assessment of binary guanosine and guanosine 5'-monophosphate (Guo/GMP) hydrogel formulations. a) Phase diagram of hydrogel printability as a function of nucleoside (Guo/GMP) and boric acid (BA) and potassium chloride (KCl) concentration after 1 h of gelation at room temperature (RT). Blue squares represent compositions that result in 3D printable hydrogels, whereas red squares represent nonprintable solutions. b) Exemplary images of binary nucleoside compositions resulting in printable (top, 100_50; 100 mM Guo and GM, 50 mM BA and KCl) and non-printable hydrogels (bottom, 70_40; 70 mM Guo and GMP, 40 mM of BA and KCl).
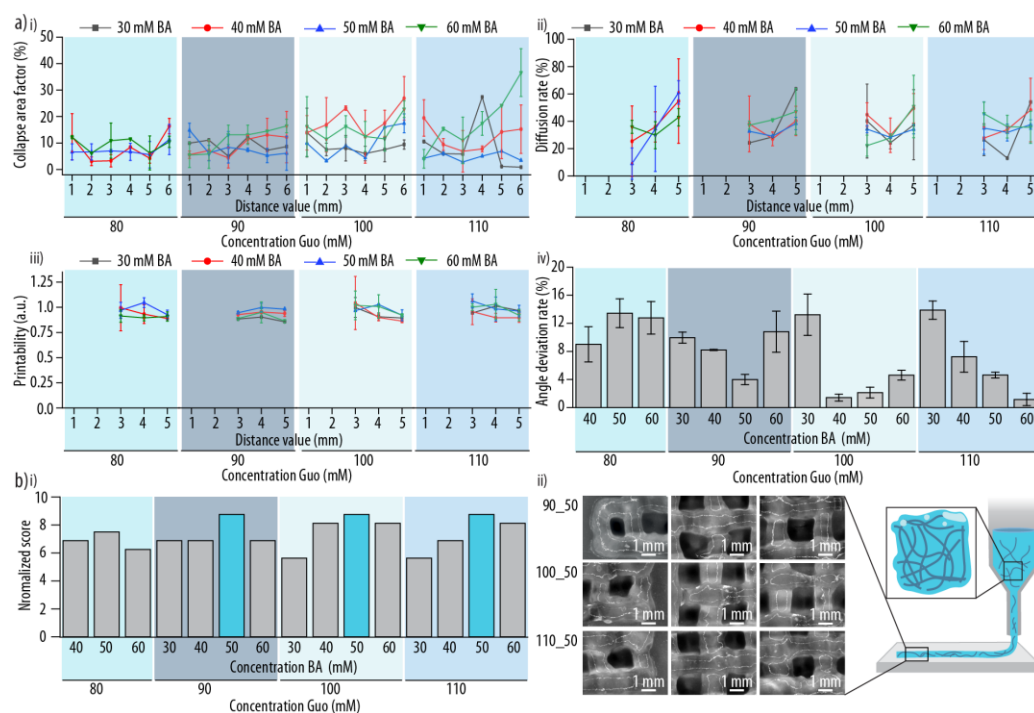
Figure 4. Identification of hydrogel compositions exhibiting optimal three dimensional (3D) printability properties by evaluating four different bioink parameters. Four different guanosine (Guo) concentrations (80, 90, 100, and 110 mM) were evaluated in a 1:1 ratio with guanosine 5'-monophosphate (GMP) and combined with four boric acid (BA) and potassium chloride (KCl) concentrations (30, 40, 50, and 60 mM). a) Results from the filament collapse and fusion tests were plotted for each of the 16 tested hydrogel compositions. The collapse area factor (i) depicts the deflection area under the printed filament, whereas the diffusion rate (ii) reflects the material spreading apparent on the printing surface. To assess printability (iii) and angle deviation rate (iv), the form and rectangularity of the printed square holes were analyzed. b) b) (i) The results of the filament fusion and collapse test were combined and then normalized to get an overall printability score. (ii) The best three hydrogel compositions, namely 90_50, 100_50, and 110_50, are illustrated by representative photos of their 3D printed corners on the left, filament cross-sections in the middle, and pores on the right. The two numbers in each composition indicate the corresponding Guo/GMP and BA/KCl concentrations, respectively. .
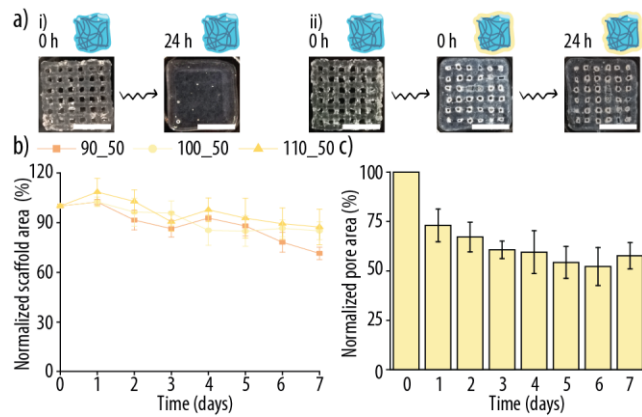
Figure 5. a) Representative images of three-dimensional (3D) printed binary guanosine and guanosine 5'-monophosphate (Guo/GMP) hydrogels (i) without and (ii) with polyethylenimine (PEI) coating after 0 and 24 h at room temperature. b) Normalized scaffold areas of printed Guo/GMP hydrogels with PEI coating (Guo/GMP-PEI hydrogel) after 7-day immersion in Advanced DMEM media at 37 °C. c) Normalized pore area of a 100_50 Guo/GMP-PEI hydrogels after 7 days of immersion in Advanced DMEM medium at 37 °C. Scale bar 10 mm.
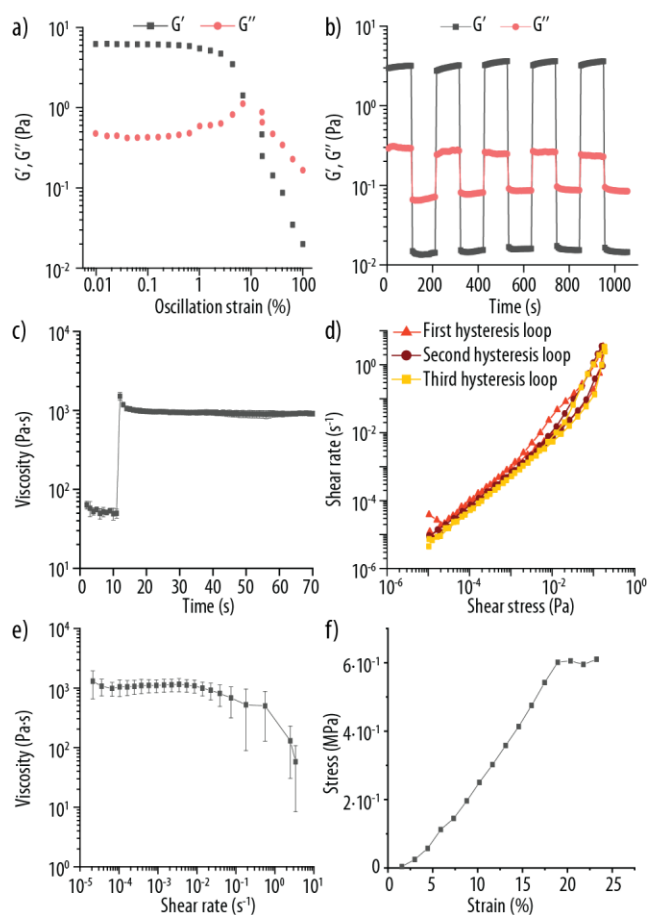
Figure 6. Rheological measurements of a binary guanosine and guanosine 5'-monophosphate hydrogels coated with hyperbranched polyethylenimine (Guo/GMP-PEI hydrogel) at 37°C. a) Guo/GMP-PEI hydrogels strain sweep test. With a fixed oscillation frequency of 1 Hz and a strain range of 0.01-100%, both the storage modulus (G') and loss modulus (G'') were measured. b) G'and G'' of Guo/GMP-PEI hydrogels measured with a strain amplitude sweep ranging from 0.1 to 100%) and a constant angular frequency of 10 rad s^{-1}. Each experimental interval was set at 100 s. c) To simulate the 3D printing scenario, first a shear rate of 3.45 s^{-1} was applied for 10 s followed by a hydrogel recovery phase at 0.1 s^{-1} for 60 s Within ~6 s, appropriate hydrogel viscosity was restored. d) Hysteresis curves of stress loading and unloading at 37 °C and a shear stress change rate of 1 Pa s^{-1}. e) Flow curve of shear thinning. f) Compressive stress-strain curve of a Guo/GMP-PEI hydrogel.
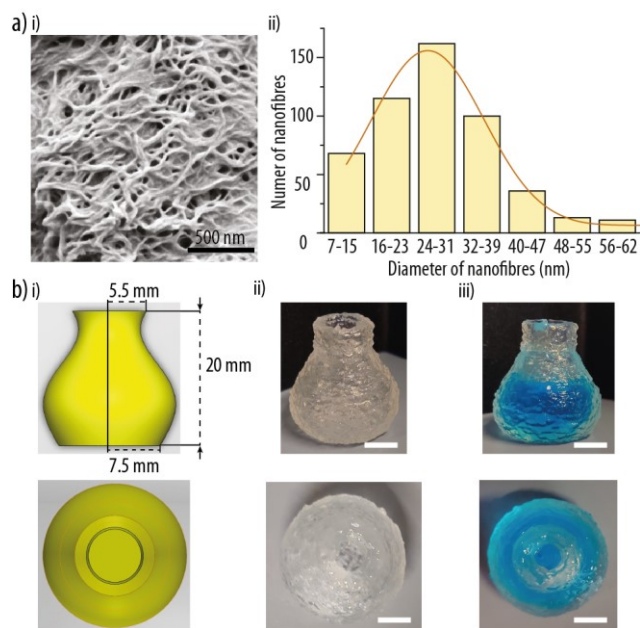
Figure 7. a) (i) Scanning electron microscopy image analysis of a binary guanosine and guanosine 5'-monophosphate (Guo/GMP) hydrogel coated with branched polyethylenimine (Guo/GMP-PEI). Hydrogel cross-section analysis revealed (i) the inner nanofibrillar hydrogel matrix and (ii) the diameter distribution histogram of the nanofibers. b) three-dimensional printing and stability testing of the developed Guo/GMP-PEI hydrogel using a jar structure. (i) First, a jar was designed in SolidWorks, then (ii) fabricated using extrusion 3D printing, and (iii) stability tested by filling the jar with dye-coloured water. Even 2 h after printing, the 3D printed jar showed no signs of structural instability and still retained all the loaded liquid. Scale bar 5 mm.
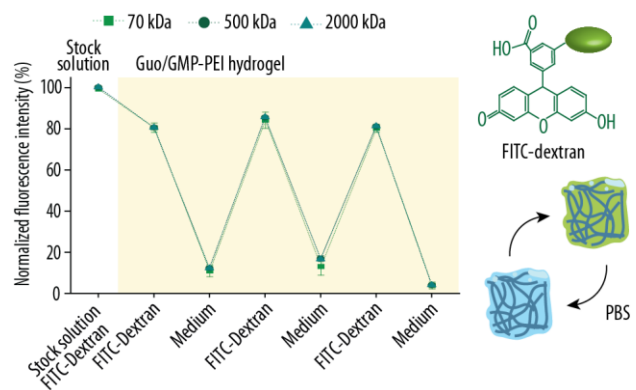
Figure 8. FITC-Dextran diffusion test through the printed hydrogel network. Normalized fluorescence intensities detected in the hydrogel are shown (λex=450 nm, λem=550 nm).
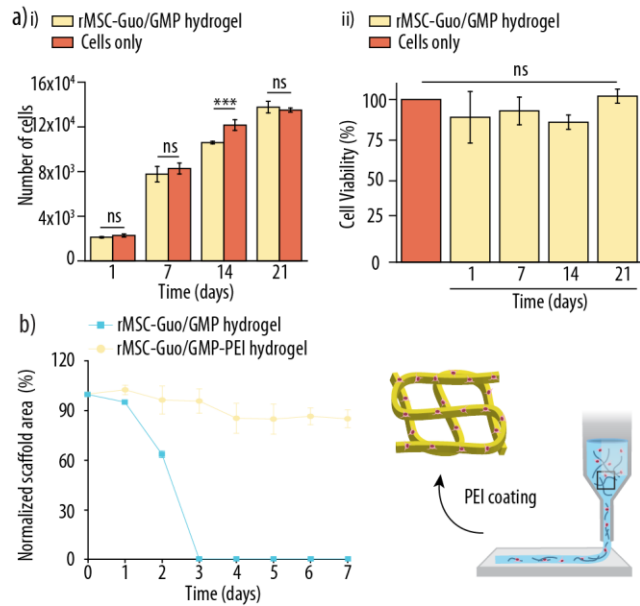
Figure 9. a) Cell proliferation (i) and viability (ii) of rat mesenchymal stem cells (rMSC) entrapped in hyperbranched polyethylenimine (PEI)-coated binary Guo/GMP hydrogels versus seeded onto tissue culture polystyrene (TCPs) plates. Cell proliferation and viability were assessed after rMSC cultivation for 1, 7, 14, and 21 days. b) Biodegradation of rMSC-Guo/GMP hydrogels with and without PEI coating. Normalized scaffold areas of 100_50 Guo/GMP (blue) and Guo/GMP-PEI hydrogels (yellow) are shown over time.
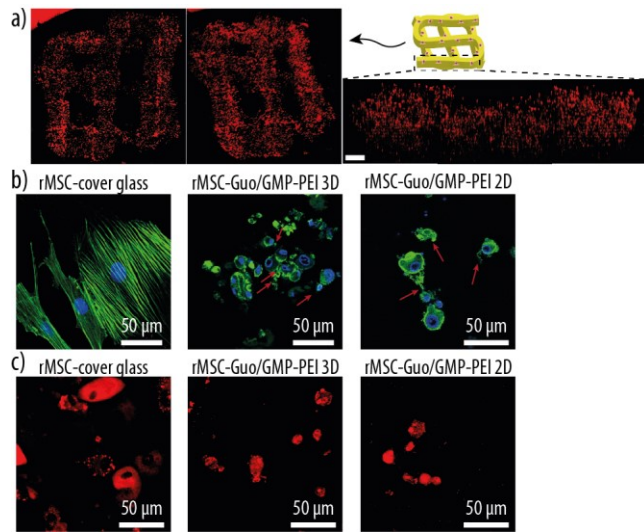
Figure 10. a) Three-dimensional (3D) representations of rat mesenchymal stem cells (rMSC; red fluorescence) entrapped in a binary guanosine and guanosine 5'-monophosphate coated with hyperbranched polyethylenimine (rMSC-Guo/GMP-PEI) hydrogels are shown after cell staining with CellTracker™ Deep Red reagent (left and middle) and 3D image of the inside filament (right) of rMSC-Guo/GMP-PEI hydrogel. b) Confocal laser scanning images of rMSCs cultivated for 21 days on cover glass (control; right), within Guo/GMP-PEI hydrogels (middle), and on top of a 2D Guo/GMP-PEI hydrogels (left). Phalloidin-Atto 488 was used for actin filament staining (green fluorescence), while DAPI was used to stain nuclei (blue fluorescence). c) Oil red O staining of adipogenically differentiated rMSCs after 21 days of incubation, with red fluorescence corresponding to lipid droplets formed in fat vacuoles.
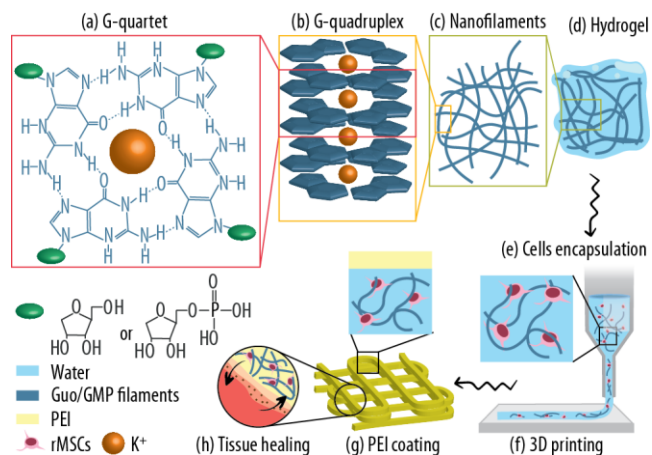
Scheme 1. Guanosine (Guo) and guanosine 5'-monophosphate salt (GMP) hydrogel formation with encapsulated rat mesenchymal stem cells (rMSCs). a) Guo/GMP hydrogel is composed by ordered structures known as Guo-quartet where a potassium ion (K^+) is located in the centrum of the cyclic planar rings. b) Four G-quartets interact by a right-handed helical structure forming a new structure known as G-quadruplex. (c) Nanofilaments are formed, consisting in the hydrogel network d). e) The assembly is mixed gently with rMSCs and all the system is three dimensional (3D) printed f). g) The scaffold is capped with a hyperbranched polyethylenimine solution (PEI) and h) will be able then to tissue healing.
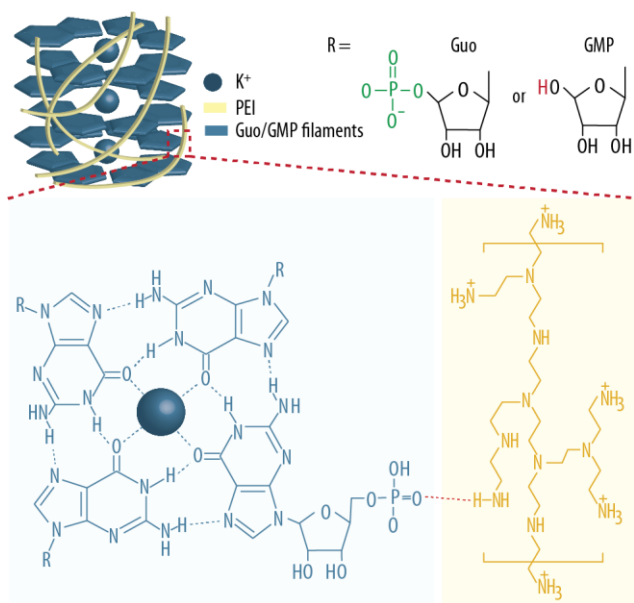
Scheme 2. Schematic illustration of the interaction between a binary guanosine and guanosine 5'-monophosphate (Guo/GMP) hydrogel and the hyperbranched polyethylenimine (PEI) coating through the GMP's phosphate groups and the –NH$_2$ groups of the PEI.

ASSOCIATED CONTENT

Supporting Information. Experimental procedure for the concentration and incubation time optimization of the hyperbranched polyethylenimine (PEI) coating, and the normalized pore areas of the obtained hydrogels. Storage modulus (G') and loss modulus (G'') of Guo/GMP hydrogels coated with hyperbranched PEI. Experimental details of the FITC-Dextran diffusion study, methodology of the rMSC incorporation into the Guo/GMP hydrogels, and confocal laser scanning microscopy images of rMSCs after incubation for 1, 3, 7 and 14 days in the hydrogels. This material is available free of charge via the Internet at http://pubs.acs.org.

AUTHOR INFORMATION

Corresponding Author

M. Godoy-Gallardo, E-mail: mgodoy@uic.es and R.A. Perez, E-mail: rperezan@uic.es

Author Contributions

The manuscript was written through contributions of all authors. All authors have given approval to the final version of the manuscript.

ACKNOWLEDGMENT

REFERENCES

(1)   Peters, G. M.; Davis, J. T. Supramolecular Gels Made from Nucleobase, Nucleoside and Nucleotide Analogs. *Chem. Soc. Rev.* **2016**, *45* (11), 3188–3206. https://doi.org/10.1039/c6cs00183a.

(2)   Du, X.; Zhou, J.; Shi, J.; Xu, B. Supramolecular Hydrogelators and Hydrogels: From Soft Matter to Molecular Biomaterials. *Chem. Rev.* **2015**, *115* (24), 13165–13307. https://doi.org/10.1021/acs.chemrev.5b00299.

(3)   Pu, F.; Ren, J.; Qu, X. Nucleobases, Nucleosides, and Nucleotides: Versatile Biomolecules for Generating Functional Nanomaterials. *Chem. Soc. Rev.* **2018**, *47* (4), 1285–1306. https://doi.org/10.1039/c7cs00673j.

(4)   Godoy-Gallardo, M.; Merino-Gómez, M.; Matiz, L. C.; Mateos-Timoneda, M. A.; Gil, F. J.; Perez, R. A. Nucleoside-Based Supramolecular Hydrogels: From Synthesis and Structural Properties to Biomedical and Tissue Engineering Applications. *ACS Biomater. Sci. Eng.* **2023**, *9* (1), 40–61. https://doi.org/10.1021/acsbiomaterials.2c01051.

(5)   Dong, R.; Pang, Y.; Su, Y.; Zhu, X. Supramolecular Hydrogels: Synthesis, Properties and Their Biomedical Applications. *Biomater. Sci.* **2015**, *3* (7), 937–954. https://doi.org/10.1039/c4bm00448e.

(6)   Zhang, Z.; He, T.; Yuan, M.; Shen, R.; Deng, L.; Yi, L.; Sun, Z.; Zhang, Y. The in Situ Synthesis of Ag/Amino Acid Biopolymer Hydrogels as Mouldable Wound Dressings. *Chem. Commun.* **2015**, *51* (87), 15862–15865. https://doi.org/10.1039/C5CC05195A.

(7)   Moreira Teixeira, L. S.; Feijen, J.; van Blitterswijk, C. A.; Dijkstra, P. J.; Karperien, M. Enzyme-Catalyzed Crosslinkable Hydrogels: Emerging Strategies for Tissue Engineering. *Biomaterials* **2012**, *33* (5), 1281–1290. https://doi.org/10.1016/j.biomaterials.2011.10.067.

(8)   Jayawarna, V.; Ali, M.; Jowitt, T. A.; Miller, A. F.; Saiani, A.; Gough, J. E.; Ulijn, R. V. Nanostructured Hydrogels for Three-Dimensional Cell Culture Through Self-Assembly of Fluorenylmethoxycarbonyl–Dipeptides. *Adv. Mater.* **2006**, *18* (5), 611–614. https://doi.org/10.1002/ADMA.200501522.

(9)   Mayr, J.; Saldías, C.; Díaz Díaz, D. Release of Small Bioactive Molecules from Physical Gels. *Chem. Soc. Rev.* **2018**, *47* (4), 1484–1515. https://doi.org/10.1039/C7CS00515F.

(10)   Huang, Z.; Li, X.; Chen, M.; Liu, Y.; Sun, X.; Song, A.; Hao, J. Guanosine-Based Thermotropic Liquid Crystals with Tunable Phase Structures and Ion-Responsive Properties. *J. Colloid Interface Sci.* **2019**, *553*, 269–279. https://doi.org/10.1016/J.JCIS.2019.06.041.

(11)   Carducci, F.; Yoneda, J. S.; Itri, R.; Mariani, P. On the Structural Stability of Guanosine-Based Supramolecular Hydrogels. *Soft Matter* **2018**, *14* (15), 2938–2948. https://doi.org/10.1039/C8SM00299A.

(12)   Zhang, J.; Li, X.; Sun, X.; Liu, Y.; Hao, J.; Tan, Y.; Song, A. G-Quadruplex Based Hydrogels Stabilized by a Cationic Polymer as an Efficient Adsorbent of Picric Acid. *New J. Chem.* **2019**, *43* (46), 18331–18338. https://doi.org/10.1039/C9NJ03143J.

(13)   Nava, G.; Carducci, F.; Itri, R.; Yoneda, J. S.; Bellini, T.; Mariani, P. Quadruplex Knots as Network Nodes: Nano-Partitioning of Guanosine Derivates in Supramolecular Hydrogels. *Soft Matter* **2019**, *15* (11), 2315–2318. https://doi.org/10.1039/C8SM02616E.

(14)   Qiao, H.; Bai, J.; Zhang, S.; Li, C. A Guanosine-Based 2-Formylphenylborate Ester Hydrogel with High Selectivity to K+ Ions. *RSC Adv.* **2020**, *10* (48), 28536–28540. https://doi.org/10.1039/D0RA05254J.

(15)   Yoneda, J. S.; de Araujo, D. R.; Sella, F.; Liguori, G. R.; Liguori, T. T. A.; Moreira, L. F.

P.; Spinozzi, F.; Mariani, P.; Itri, R. Self-Assembled Guanosine-Hydrogels for Drug-Delivery Application: Structural and Mechanical Characterization, Methylene Blue Loading and Controlled Release. *Mater. Sci. Eng. C* **2021**, *121*, 111834. https://doi.org/10.1016/J.MSEC.2020.111834.

(16)   Merino-Gómez, M.; Gil, J.; Perez, R. A.; Godoy-Gallardo, M. Polydopamine Incorporation Enhances Cell Differentiation and Antibacterial Properties of 3D-Printed Guanosine-Borate Hydrogels for Functional Tissue Regeneration. *Int. J. Mol. Sci.* **2023**, *24* (4), 4224. https://doi.org/https://doi.org/10.3390/ijms24044224.

(17)   Merino-Gómez, M.; Godoy-Gallardo, M.; Wendner, M.; Mateos-Timoneda, M. A.; Gil, F. J.; Perez, R. A. Optimization of Guanosine-Based Hydrogels with Boric Acid Derivatives for Enhanced Long-Term Stability and Cell Survival. *Front. Bioeng. Biotechnol.* **2023**, *11*, 1147943. https://doi.org/10.3389/FBIOE.2023.1147943.

(18)   Ghosh, A.; Parasar, B.; Bhattacharyya, T.; Dash, J. Chiral Carbon Dots Derived from Guanosine 5′-Monophosphate Form Supramolecular Hydrogels. *Chem. Commun.* **2016**, *52* (74), 11159–11162. https://doi.org/10.1039/C6CC05947C.

(19)   Plank, T. N.; Skala, L. P.; Davis, J. T. Supramolecular Hydrogels for Environmental Remediation: G4-Quartet Gels That Selectively Absorb Anionic Dyes from Water. *Chem. Commun.* **2017**, *53* (46), 6235–6238. https://doi.org/10.1039/C7CC03118A.

(20)   Li, Y.; Liu, Y.; Ma, R.; Xu, Y.; Zhang, Y.; Li, B.; An, Y.; Shi, L. A G-Quadruplex Hydrogel via Multicomponent Self-Assembly: Formation and Zero-Order Controlled Release. *ACS Appl. Mater. Interfaces* **2017**, *9* (15), 13056–13067. https://doi.org/10.1021/ACSAMI.7B00957/SUPPL_FILE/AM7B00957_SI_001.PDF.

(21)   Bhattacharyya, T.; Saha, P.; Dash, J. Guanosine-Derived Supramolecular Hydrogels:

Recent Developments and Future Opportunities. *ACS Omega* **2018**, *3* (2), 2230–2241. https://doi.org/10.1021/ACSOMEGA.7B02039/ASSET/IMAGES/LARGE/AO-2017-02039G_0011.JPEG.

(22)   Pieraccini, S.; Campitiello, M.; Carducci, F.; Davis, J. T.; Mariani, P.; Masiero, S. Playing Supramolecular Dominoes with Light: Building and Breaking a Photoreversible G-Quadruplex Made from Guanosine, Boric Acid and an Azobenzene. *Org. Biomol. Chem.* **2019**, *17* (10), 2759–2769. https://doi.org/10.1039/C9OB00193J.

(23)   Plank, T. N.; Davis, J. T. A G4·K+ Hydrogel That Self-Destructs. *Chem. Commun.* **2016**, *52* (28), 5037–5040. https://doi.org/10.1039/C6CC01494A.

(24)   GM, P.; LP, S.; JT, D. A Molecular Chaperone for G4-Quartet Hydrogels. *J. Am. Chem. Soc.* **2016**, *138* (1), 134–139. https://doi.org/10.1021/JACS.5B08769.

(25)   Biswas, A.; Malferrari, S.; Kalaskar, D. M.; Das, A. K. Arylboronate Esters Mediated Self-Healable and Biocompatible Dynamic G-Quadruplex Hydrogels as Promising 3D-Bioinks. *Chem. Commun.* **2018**, *54* (14), 1778–1781. https://doi.org/10.1039/C7CC09051J.

(26)   Li, J.; Wei, H.; Peng, Y.; Geng, L.; Zhu, L.; Cao, X. Y.; Liu, C. Sen; Pang, H. A Multifunctional Self-Healing G-PyB/KCl Hydrogel: Smart Conductive, Rapid Room-Temperature Phase-Selective Gelation, and Ultrasensitive Detection of Alpha-Fetoprotein. *Chem. Commun.* **2019**, *55* (55), 7922–7925. https://doi.org/10.1039/c9cc02770j.

(27)   Bhattacharyya, T.; Kumar, Y. P.; Dash, J. Supramolecular Hydrogel Inspired from DNA Structures Mimics Peroxidase Activity. *ACS Biomater. Sci. Eng.* **2017**, *3* (10), 2358–2365. https://doi.org/10.1021/acsbiomaterials.7b00563.

(28)   Peters, G. M.; Skala, L. P.; Plank, T. N.; Hyman, B. J.; Manjunatha Reddy, G. N.; Marsh, A.; Brown, S. P.; Davis, J. T. A G4·K+ Hydrogel Stabilized by an Anion. *J. Am. Chem.*

Soc. **2014**, *136* (36), 12596–12599. https://doi.org/10.1021/ja507506c.

(29)   Kumar, A.; Gupta, S. K. Synthesis of 5′-GMP-Mediated Porous Hydrogel Containing β-FeOOH Nanostructures: Optimization of Its Morphology, Optical and Magnetic Properties. *J. Mater. Chem. B* **2013**, *1* (42), 5818–5830. https://doi.org/10.1039/C3TB20877J.

(30)   Kwan, I. C. M.; Delley, R. J.; Hodgson, D. R. W.; Wu, G. Single Atom Modification Leads to Enhanced Nucleotide Self-Assembly: The Role of Cation Bridging. *Chem. Commun.* **2011**, *47* (13), 3882–3884. https://doi.org/10.1039/C0CC05654E.

(31)   Sreenivasachary, N.; Lehn, J. M. Gelation-Driven Component Selection in the Generation of Constitutional Dynamic Hydrogels Based on Guanine-Quartet Formation. *Proc. Natl. Acad. Sci. U. S. A.* **2005**, *102* (17), 5938–5943. https://doi.org/10.1073/pnas.0501663102.

(32)   Belda, R.; García-España, E.; Morris, G. A.; Steed, J. W.; Aguilar, J. A. Guanosine-5'-Monophosphate Polyamine Hybrid Hydrogels: Enhanced Gel Strength Probed by z-Spectroscopy. *Chemistry* **2017**, *23* (32), 7755–7760. https://doi.org/10.1002/CHEM.201700642.

(33)   Wang, C.; Huang, W.; Zhou, Y.; He, L.; He, Z.; Chen, Z.; He, X.; Tian, S.; Liao, J.; Lu, B.; Wei, Y.; Wang, M. 3D Printing of Bone Tissue Engineering Scaffolds. *Bioact. Mater.* **2020**, *5* (1), 82–91. https://doi.org/10.1016/j.bioactmat.2020.01.004.

(34)   Levato, R.; Jungst, T.; Scheuring, R. G.; Blunk, T.; Groll, J.; Malda, J. From Shape to Function: The Next Step in Bioprinting. *Adv. Mater.* **2020**, *32* (12), 1906423. https://doi.org/10.1002/ADMA.201906423.

(35)   Bhattacharyya, A.; Janarthanan, G.; Noh, I. Nano-Biomaterials for Designing Functional Bioinks towards Complex Tissue and Organ Regeneration in 3D Bioprinting. *Addit. Manuf.* **2021**, *37*, 101639. https://doi.org/10.1016/J.ADDMA.2020.101639.

(36) Lee, J. M.; Ng, W. L.; Yeong, W. Y. Resolution and Shape in Bioprinting: Strategizing towards Complex Tissue and Organ Printing. *Appl. Phys. Rev.* **2019**, *6* (1), 011307. https://doi.org/10.1063/1.5053909.

(37) Ashammakhi, N.; Ahadian, S.; Xu, C.; Montazerian, H.; Ko, H.; Nasiri, R.; Barros, N.; Khademhosseini, A. Bioinks and Bioprinting Technologies to Make Heterogeneous and Biomimetic Tissue Constructs. *Mater. Today Bio* **2019**, *1*. https://doi.org/10.1016/j.mtbio.2019.100008.

(38) Ng, W. L.; Chua, C. K.; Shen, Y. F. Print Me An Organ! Why We Are Not There Yet. *Prog. Polym. Sci.* **2019**, *97*, 101145. https://doi.org/10.1016/J.PROGPOLYMSCI.2019.101145.

(39) Malda, J.; Visser, J.; Melchels, F. P.; Jüngst, T.; Hennink, W. E.; Dhert, W. J. A.; Groll, J.; Hutmacher, D. W. 25th Anniversary Article: Engineering Hydrogels for Biofabrication. *Adv. Mater.* **2013**, *25* (36), 5011–5028. https://doi.org/10.1002/ADMA.201302042.

(40) Guo, K.; Wang, H.; Li, S.; Zhang, H.; Li, S.; Zhu, H.; Yang, Z.; Zhang, L.; Chang, P.; Zheng, X. Collagen-Based Thiol-Norbornene Photoclick Bio-Ink with Excellent Bioactivity and Printability. *ACS Appl. Mater. Interfaces* **2021**, *13* (6), 7037–7050. https://doi.org/10.1021/acsami.0c16714.

(41) Suntornnond, R.; Ng, W. L.; Huang, X.; Yeow, C. H. E.; Yeong, W. Y. Improving Printability of Hydrogel-Based Bio-Inks for Thermal Inkjet Bioprinting Applications via Saponification and Heat Treatment Processes. *J. Mater. Chem. B* **2022**, *10* (31), 5989–6000. https://doi.org/10.1039/D2TB00442A.

(42) Jiang, T.; Munguia-Lopez, J. G.; Flores-Torres, S.; Kort-Mascort, J.; Kinsella, J. M. Extrusion Bioprinting of Soft Materials: An Emerging Technique for Biological Model Fabrication. *Appl. Phys. Rev.* **2019**, *6* (1), 011310. https://doi.org/10.1063/1.5059393.

(43) Ng, W. L.; Lee, J. M.; Zhou, M.; Chen, Y. W.; Lee, K. X. A.; Yeong, W. Y.; Shen, Y. F. Vat Polymerization-Based Bioprinting—Process, Materials, Applications and Regulatory Challenges. *Biofabrication* **2020**, *12* (2), 022001. https://doi.org/10.1088/1758-5090/AB6034.

(44) Li, X.; Liu, B.; Pei, B.; Chen, J.; Zhou, D.; Peng, J.; Zhang, X.; Jia, W.; Xu, T. Inkjet Bioprinting of Biomaterials. *Chem. Rev.* **2020**, *120* (19), 10793–10833. https://doi.org/10.1021/acs.chemrev.0c00008.

(45) Biswas, A.; Malferrari, S.; Kalaskar, D. M.; Das, A. K. Arylboronate Esters Mediated Self-Healable and Biocompatible Dynamic G-Quadruplex Hydrogels as Promising 3D-Bioinks. *Chem. Commun.* **2018**, *54* (14), 1778–1781. https://doi.org/10.1039/c7cc09051j.

(46) Böhm, I.; Kreth, S. K.; Ritter, H. Hyperbranched Polyethylenimine Bearing Cyclodextrin Moieties Showing Temperature and PH Controlled Dye Release. *Beilstein J. Org. Chem* **2011**, *7*, 1130–1134. https://doi.org/10.3762/bjoc.7.130.

(47) Forrest, M. L.; Gabrielson, N.; Pack, D. W. Cyclodextrin–Polyethylenimine Conjugates for Targeted in Vitro Gene Delivery. *Biotechnol. Bioeng.* **2005**, *89* (4), 416–423. https://doi.org/10.1002/BIT.20356.

(48) Maciollek, A.; Munteanu, M.; Ritter, H. New Generation of Polymeric Drugs: Copolymer from NIPAAM and Cyclodextrin Methacrylate Containing Supramolecular-Attached Antitumor Derivative. *Macromol. Chem. Phys.* **2010**, *211* (2), 245–249. https://doi.org/10.1002/MACP.200900436.

(49) Zhou, J.; Ritter, H. Cyclodextrin Functionalized Polymers as Drug Delivery Systems. *Polym. Chem.* **2010**, *1* (10), 1552–1559. https://doi.org/10.1039/C0PY00219D.

(50) Schneider, C. A.; Rasband, W. S.; Eliceiri, K. W. NIH Image to ImageJ: 25 Years of Image

Analysis. *Nat. Methods* **2012**, *9* (7), 671–675. https://doi.org/10.1038/nmeth.2089.

(51)   Ribeiro, A.; Blokzijl, M. M.; Levato, R.; Visser, C. W.; Castilho, M.; Hennink, W. E.; Vermonden, T.; Malda, J. Assessing Bioink Shape Fidelity to Aid Material Development in 3D Bioprinting. *Biofabrication* **2018**, *10* (1). https://doi.org/10.1088/1758-5090/aa90e2.

(52)   Habib, A.; Sathish, V.; Mallik, S.; Khoda, B. 3D Printability of Alginate-Carboxymethyl Cellulose Hydrogel. *Materials (Basel).* **2018**, *11* (3). https://doi.org/10.3390/ma11030454.

(53)   Habib, M. A.; Khoda, B. Development of Clay Based Novel Bio-Ink for 3D Bio-Printing Process. *Procedia Manuf.* **2018**, *26*, 846–856. https://doi.org/10.1016/J.PROMFG.2018.07.105.

(54)   Sandrin, D.; Wagner, D.; Sitta, C. E.; Thoma, R.; Felekyan, S.; Hermes, H. E.; Janiak, C.; De Sousa Amadeu, N.; Kühnemuth, R.; Löwen, H.; Egelhaaf, S. U.; Seidel, C. A. M. Diffusion of Macromolecules in a Polymer Hydrogel: From Microscopic to Macroscopic Scales. *Phys. Chem. Chem. Phys.* **2016**, *18* (18), 12860–12876. https://doi.org/10.1039/c5cp07781h.

(55)   Lopera, A.; Aguilar, J. A.; Belda, R.; Verdejo, B.; Steed, J. W.; García-España, E. Hybrid GMP–Polyamine Hydrogels as New Biocompatible Materials for Drug Encapsulation. *Soft Matter* **2020**, *16* (28), 6514–6522. https://doi.org/10.1039/D0SM00704H.

(56)   Ghosh, T.; Biswas, A.; Gavel, P. K.; Das, A. K. Engineered Dynamic Boronate Ester-Mediated Self-Healable Biocompatible G-Quadruplex Hydrogels for Sustained Release of Vitamins. *Langmuir* **2020**, *36* (6), 1574–1584. https://doi.org/10.1021/acs.langmuir.9b03837.

(57)   Biswas, A.; Ghosh, T.; Gavel, P. K.; Das, A. K. PEG Functionalized Stimuli Responsive Self-Healable Injectable Dynamic Imino-Boronate G-Quadruplex Hydrogel for the

Delivery of Doxorubicin. *ACS Appl. Bio Mater.* **2020**, *3* (2), 1052–1060. https://doi.org/10.1021/ACSABM.9B01034.

(58)   Kruse, C. R.; Singh, M.; Targosinski, S.; Sinha, I.; Sørensen, J. A.; Eriksson, E.; Nuutila, K. The Effect of PH on Cell Viability, Cell Migration, Cell Proliferation, Wound Closure, and Wound Reepithelialization: In Vitro and in Vivo Study. *Wound Repair Regen.* **2017**, *25* (2), 260–269. https://doi.org/10.1111/wrr.12526.

(59)   Yilmaz, B.; Al Rashid, A.; Mou, Y. A.; Evis, Z.; Koç, M. Bioprinting: A Review of Processes, Materials and Applications. *Bioprinting* **2021**, *23*, e00148. https://doi.org/10.1016/J.BPRINT.2021.E00148.

(60)   Ouyang, L.; Yao, R.; Zhao, Y.; Sun, W. Effect of Bioink Properties on Printability and Cell Viability for 3D Bioplotting of Embryonic Stem Cells. *Biofabrication* **2016**, *8* (3). https://doi.org/10.1088/1758-5090/8/3/035020.

(61)   Wu, D.; Yu, Y.; Tan, J.; Huang, L.; Luo, B.; Lu, L.; Zhou, C. 3D Bioprinting of Gellan Gum and Poly (Ethylene Glycol) Diacrylate Based Hydrogels to Produce Human-Scale Constructs with High-Fidelity. *Mater. Des.* **2018**, *160*, 486–495. https://doi.org/10.1016/j.matdes.2018.09.040.

(62)   Stichler, S.; Jungst, T.; Schamel, M.; Zilkowski, I.; Kuhlmann, M.; Böck, T.; Blunk, T.; Teßmar, J.; Groll, J. Thiol-Ene Clickable Poly(Glycidol) Hydrogels for Biofabrication. *Ann. Biomed. Eng.* **2017**, *45* (1), 273–285. https://doi.org/10.1007/s10439-016-1633-3.

(63)   Lee, H. J.; Kim, Y. B.; Ahn, S. H.; Lee, J. S.; Jang, C. H.; Yoon, H.; Chun, W.; Kim, G. H. A New Approach for Fabricating Collagen/ECM-Based Bioinks Using Preosteoblasts and Human Adipose Stem Cells. *Adv. Healthc. Mater.* **2015**, *4* (9), 1359–1368. https://doi.org/10.1002/adhm.201500193.

(64) Yildirimkaraman, O.; Özenler, S.; Gunay, U. S.; Durmaz, H.; Ylldlz, Ü. H. Electroactive Nanogel Formation by Reactive Layer-by-Layer Assembly of Polyester and Branched Polyethylenimine via Aza-Michael Addition. *Langmuir* **2021**, *37* (37), 10902–10913. https://doi.org/10.1021/acs.langmuir.1c01070.

(65) Chen, C.; Chen, F.; Liu, L.; Zhao, J.; Wang, F. Cross-Linked Hyperbranched Polyethylenimine as an Efficient Multidimensional Binder for Silicon Anodes in Lithium-Ion Batteries. *Electrochim. Acta* **2019**, *326*, 134964. https://doi.org/10.1016/J.ELECTACTA.2019.134964.

(66) Saengow, C.; Giacomin, A. J.; Grizzuti, N.; Pasquino, R. Startup Steady Shear Flow from the Oldroyd 8-Constant Framework. *Phys. Fluids* **2019**, *31* (6), 063101. https://doi.org/10.1063/1.5091493.

(67) Guo, L. P.; Han, X.; Lei, Y.; Wang, L.; Yu, P. F.; Shi, S. Study on the Thixotropy and Structural Recovery Characteristics of Waxy Crude Oil Emulsion. *Pet. Sci.* **2021**, *18* (4), 1195–1202. https://doi.org/10.1016/J.PETSCI.2021.07.003.

(68) Axpe, E.; Chan, D.; Offeddu, G. S.; Chang, Y.; Merida, D.; Hernandez, H. L.; Appel, E. A. A Multiscale Model for Solute Diffusion in Hydrogels. *Macromolecules* **2019**, *52* (18), 6889–6897. https://doi.org/10.1021/acs.macromol.9b00753.

(69) Lanznaster, D.; Dal-Cim, T.; Piermartiri, T. C. B.; Tasca, C. I. Guanosine: A Neuromodulator with Therapeutic Potential in Brain Disorders. *Aging Dis.* **2016**, *7* (5), 657–679. https://doi.org/10.14336/AD.2016.0208.

(70) Massari, C. M.; Zuccarini, M.; Di Iorio, P.; Tasca, C. I. Guanosine Mechanisms of Action: Toward Molecular Targets. *Front. Pharmacol.* **2021**, *12*. https://doi.org/10.3389/FPHAR.2021.653146.

(71)   Cidonio, G.; Glinka, M.; Dawson, J. I.; Oreffo, R. O. C. The Cell in the Ink: Improving Biofabrication by Printing Stem Cells for Skeletal Regenerative Medicine. *Biomaterials* **2019**, *209*, 10–24. https://doi.org/10.1016/J.BIOMATERIALS.2019.04.009.

(72)   Cavo, M.; Caria, M.; Pulsoni, I.; Beltrame, F.; Fato, M.; Scaglione, S. A New Cell-Laden 3D Alginate-Matrigel Hydrogel Resembles Human Breast Cancer Cell Malignant Morphology, Spread and Invasion Capability Observed "in Vivo." *Sci. Rep.* **2018**, *8* (1), 1–12. https://doi.org/10.1038/s41598-018-23250-4.

(73)   Kenny, P. A.; Lee, G. Y.; Myers, C. A.; Neve, R. M.; Semeiks, J. R.; Spellman, P. T.; Lorenz, K.; Lee, E. H.; Barcellos-Hoff, M. H.; Petersen, O. W.; Gray, J. W.; Bissell, M. J. The Morphologies of Breast Cancer Cell Lines in Three-Dimensional Assays Correlate with Their Profiles of Gene Expression. *Mol. Oncol.* **2007**, *1* (1), 84–96. https://doi.org/10.1016/J.MOLONC.2007.02.004.

(74)   Cofiño, C.; Perez-Amodio, S.; Semino, C. E.; Engel, E.; Mateos-Timoneda, M. A. Development of a Self-Assembled Peptide/Methylcellulose-Based Bioink for 3D Bioprinting. *Macromol. Mater. Eng.* **2019**, *304* (11), 1900353. https://doi.org/10.1002/MAME.201900353.

(75)   Sun, Z.; Gong, J.; Wu, L.; Li, P. Imaging Lipid Droplet Fusion and Growth. *Methods Cell Biol.* **2013**, *116*, 253–268. https://doi.org/10.1016/B978-0-12-408051-5.00013-9.

GRAPHICAL ABSTRACT
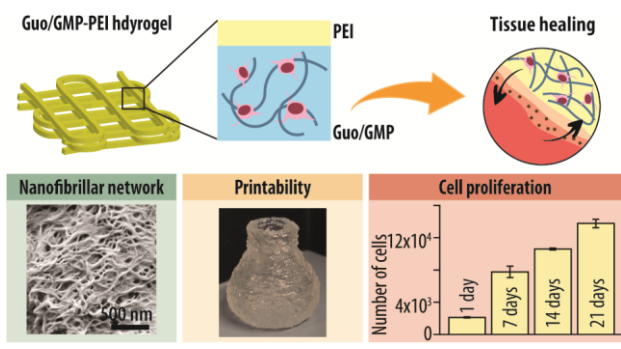
Supporting Information

Advanced binary guanosine and guanosine 5'-monophosphate cell-laden hydrogels for soft tissue reconstruction by 3D bioprinting.

Maria Godoy-Gallardo[†,]*, Maria Merino-Gómez[†], Miguel A. Mateos-Timoneda[†],

Ulrich Eckhard[#], F. Javier Gil[†], Roman A. Perez[†,]*

[†]Bioengineering Institute of Technology (BIT), International University of Catalonia (UIC), Carrer de Josep Trueta, 08195, Sant Cugat del Vallès, Barcelona, Spain

[#]Department of Structural and Molecular Biology, Molecular Biology Institute of Barcelona (IBMB), Higher Scientific Research Council (CSIC), Barcelona Science Park, Baldiri Reixac 15-21, 08028 Barcelona, Spain.

Corresponding Author. M. Godoy-Gallardo, E-mail: mgodoy@uic.es and R.A. Perez, E-mail: rperezan@uic.es

Table S1. The score attributed to the value-ranges derived for the collapse area factor, diffusion rate, printability, and angle deviation rate is shown in the left column. Reprinted with permission from Frontiers in Bioengineering and Biotechnology (Merino-Gómez et al. *Front. Bioeng. Biotechnol.* **2023**, 11, 1147943).

Score	Collapse area factor (C_f)	Diffusion rate (Df_r)	Printability (P_r)	Angle deviation rate (D_a)
2	96 – 100%	96 – 100%	0.00 – 0.05	96 – 100%
4	90 – 95%	90 – 95%	0.05 – 0.10	90 – 95%
6	85 – 90%	85 – 90%	0.10 – 0.15	85 – 90%
8	80 – 85%	80 – 85%	0.15 – 0.20	80 – 85%
10	75 – 80%	75 – 80%	0.20 – 0.25	75 – 80%
12	70 – 75%	70 – 75%	0.25 – 0.30	70 – 75%
14	65 – 70%	65 – 70%	0.30 – 0.35	65 – 70%
16	60 – 65%	60 – 65%	0.35 – 0.40	60 – 65%
18	55 – 60%	55 – 60%	0.40 – 0.45	55 – 60%
20	50 – 55%	50 – 55%	0.45 – 0.50	50 – 55%
22	45 – 50%	45 – 50%	0.50 – 0.55	45 – 50%
24	40 – 45%	40 – 45%	0.55 – 0.60	40 – 45%
26	35 – 40%	35 – 40%	0.60 – 0.65	35 – 40%
28	30 – 35%	30 – 35%	0.65 – 0.70	30 – 35%
30	25 – 30%	25 – 30%	0.70 – 0.75	25 – 30%
32	20 – 25%	20 – 25%	0.75 – 0.80	20 – 25%
34	15 – 20%	15 – 20%	0.80 – 0.85	15 – 20%
36	10 – 15%	10 – 15%	0.85 – 0.90	10 – 15%
38	5 – 10%	5 – 10%	0.90 – 0.95	5 – 10%
40	0 – 5%	0 – 5%	0.95 – 1.00	0 – 5%

PEI Optimization

A set of hyperbranched polyethylenimine (PEI) solutions (0.5, 1.0, 5 and 10 mg mL^{-1}) were prepared to immerse printed guanosine/guanosine 5'-monophosphate (Guo/GMP) hydrogels (100 mM of Guo and GMP; 50 mM of potassium chloride (KCl) and boric acid (BA) solution) in a 6 well-plate to improve the stability of the bioink. The systems were incubated at 37°C for different time points (5, 15, 30 and 60 min). Then, the samples were washed three times in phosphate buffered saline (PBS) and hydrogel spreading was monitored at room temperature (RT). The morphology of the printed hydrogels was followed over time by taking pictures and measuring the area of both the enclosed holes (Figure S1a) and the printed scaffolds (Figure S1b) by ImageJ software.[35]

Figure S1a shows a control experiment in which the Guo/GMP hydrogel totally spreads after 1 day at RT, resulting in total disappearance of the holes. The results (S1b-1e) demonstrated that treatment with 5 and 10 mg mL^{-1} PEI solutions were superior over 1.0 and 0.5 mg mL^{-1} PEI solutions, as they allowed to maintain the shape of the printed holes independently of the incubation time. Importantly, as both PEI concentrations showed the same effect on hydrogel stability of the hydrogel, we selected the 5 mg mL^{-1} PEI solution and 15 min of incubation at 37°C for our subsequent experiments.
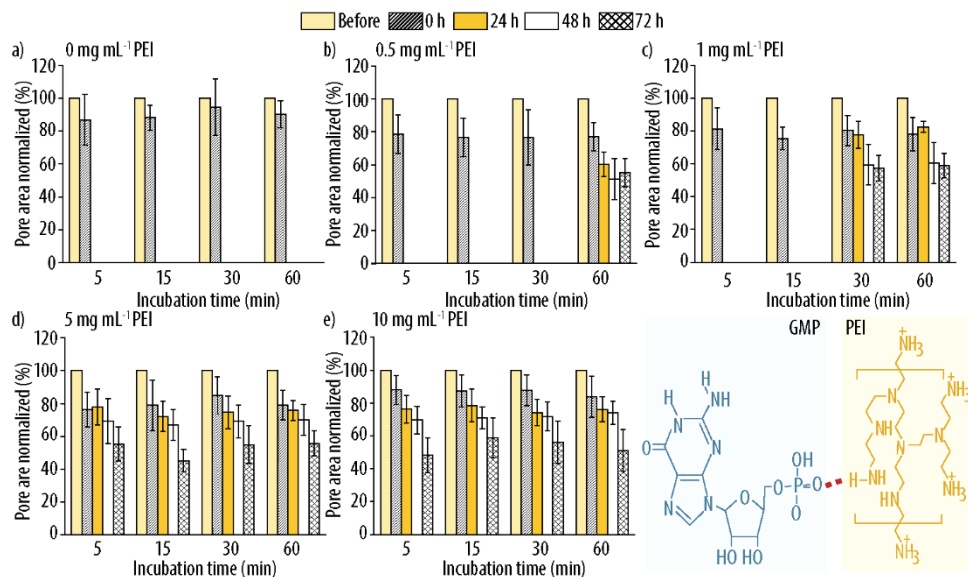
Figure S1. Normalized pore areas of the Guo/GMP hydrogels (100 mM Guo and GMP; 50 mM KCl and BA) after immersion into PEI solutions at different concentrations and incubation times. PEI concentrations used were a) 0.0, b) 0.5, c) 1.0, d) 5, and e) 10 mg mL^{-1}, and incubation was performed for four different time points (5, 15, 30 and 60 min) at 37°C.

FITC-Dextran incubation time

Guo/GMP-PEI scaffolds were printed in a 6-well plate, loaded with 4 mL of three different fluorescein isothiocyanate (FITC)-Dextran (70, 500 or 2000 kDa) solutions at a concentration of 1 mg mL^{-1} and incubated at 37°C. At different time points, 100 μL of the supernatant were transferred to a new 96-well plate and the fluorescence intensity (λex=450 nm, λem=550 nm) was measured using a multimode plate reader (Infinite M Nano, TECAN, Switzerland).

Figure S3 shows that barely any change in fluorescence intensity was observed after 8h of incubation of the printed hydrogels in the tested FITC-dextran solutions (70, 500 and 2000 kDa), indicating fast uptake independent of the dextran molecular weight. Note, measured intensities were normalized to the initial fluorescence signal of the FITC-dextran solutions to improve comparability, and the FITC-dextran uptake was monitored for 48 hours. Notably, no difference in normalized fluorescence intensity was observed for the different FITC-dextran molecular weights, and 8 hours of incubation seemed sufficient for full gel loading. Thus we selected an incubation time of 10 h for the final hydrogel diffusion test.
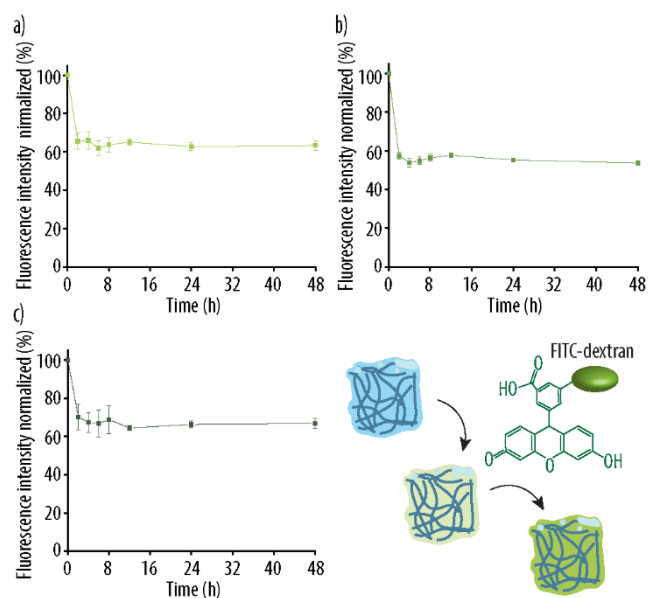
Figure S2. Normalized fluorescence intensity readings (λex=450 nm, λem=550 nm) of the hydrogel supernatants after incubation with solutions of 1 mg mL^{-1} of a) 70 kDa, b) 500 kDa, and c) 2000 kDa FITC-Dextran. Uptake into the hydrogel was monitored indirectly over a total of 48 hours by measuring the fluorescent signal of the surrounding solution.

Incorporation of rMSC into the Guo/GMP-PEI hydrogels

We tested various mixing protocols to ensure optimal cell entrapment into the hydrogel matrix. For that purpose, Guo/GMP hydrogels were prepared as described in section 2.3 but under sterile conditions, and kept at 37 °C. Then, 750 µL of the hydrogel were transferred into a new syringe and 50 µL of a rMSC suspension (10^6 cells in 150 µL complete medium, 37 °C) containing a blue food colorant (Dr. Oetker) was added. The process was repeated until three layers of rat mesenchymal cells (rMSC) were added and a final layer of 750 µL of Guo/GMP hydrogel was deposited. Next, the hydrogel and cell solutions were trespassed gently between two syringes that were kept at 37 °C using a metal block. Incresased mixing was monitored over different numbers of passages. As evident in Figure S4, after 6 passaged the mixture appears well mixed and a higher number of passages does not further improve the homogeneity of the cell loaded hydrogel.
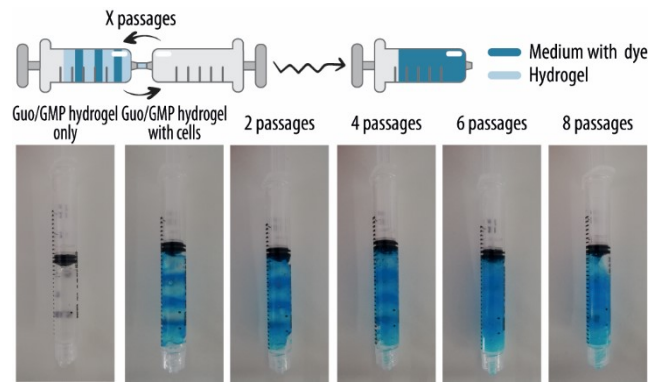
Figure S3. Formulation of cell laden Guo/GMP hydrogels. Schematic of mixing rMSC containing a blue food colorant into a Guo/GMP hydrogel solution using a two-syringe set-up and keeping all solutions at 37 °C using a metal block. Six passages from syringe 1 to syringe 2 ensured homogenous mixing of the two solutions. Note, the food dye was solely used for monitoring and optimizing the mixing process but was omitted in subsequent experiments.
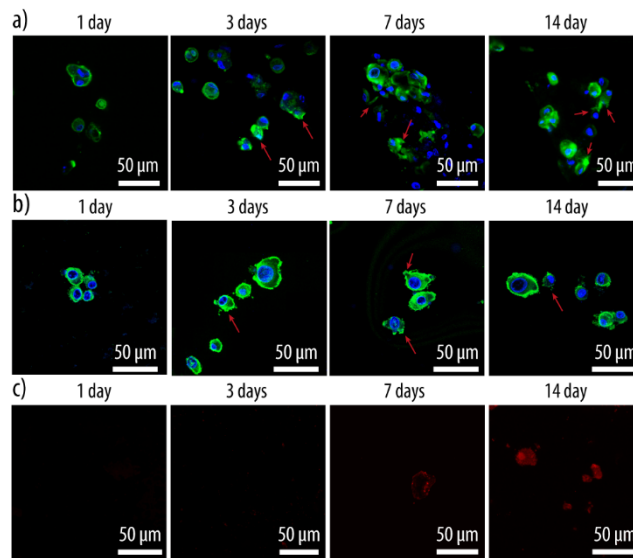
Figure S4. a) Merged confocal laser scanning images of 3D rMSC entrapped in Guo/GMP-PEI (rMSC-Guo/GMP-PEI) hydrogels after 1, 3, 7 and 14 days of incubation are shown using phalloidin-Atto 488 (green fluorescence signal) and DAPI (blue fluorescence signal) to label actin filaments and nuclei, respectively. b) Merged confocal laser scanning images of rMSCs cultured onto a 2D Guo/GMP-PEI hydrogels after 1, 3, 7 and 14 days of incubation. c) Oil red O staining of adipogenically induced rMSCs after 1, 3, 7 and 14 days of incubation. Red fluorescence signal corresponds to lipid droplet formation and indicates successful cell differentiation.